Master of Science Thesis

Monte Carlo based investigation of the influence of accelerator-head geometry on megavolt photon beam quality in radiotherapy.

By
Beatrice Jutemark

Supervisors: Lasse Rye Aarup and Håkan Nyström

Department of Medical Radiation Physics
The Jubileum Institute

Lund University, 2005

LUJI-RADFY-EX-1/2005

Abstract

This project concerns the precise characterization of one of the VARIAN accelerators used in the radiotherapy clinic at the Finsen Centre at Copenhagen University Hospital, Denmark.

Detailed characteristics of the clinical beam incident on the patient are almost impossible to measure. Even though manufacturers provide the necessary information about the specific accelerator, the models are constantly improving and the individual purchasers often adjust the machines to match e.g. the characteristics of a previous or of an existing accelerator. One particular concern is that it is impossible to get accurate information about the primary electron beam, such as its energy and its radial intensity distribution, as it leaves the accelerator vacuum window and hits the bremsstrahlung target. With the Monte Carlo technique it is possible to simulate the radiation transport through the accelerator head and achieve a better understanding of the clinical beam. The accuracy of the simulated beams were validated by the agreement with measured dose distributions.

In this project the photon beams from a Varian Clinac-23EX accelerator were investigated. This was done by simulating 6 and 18 MV photon beams for two different field sizes, 10 x 10 cm^2 and 40 x 40 cm^2, using the BEAMnrc and the DOSXYZnrc Monte Carlo code system. The linac geometry was used as input to the Monte Carlo code with specifications obtained from the vendor of the accelerator. Total dose measurements were performed in water using a Scanditronix-Wellhöfer RFA-300 beam scanner with an RK-8305 ionization chamber.

To validate the Monte Carlo model for the photon-beam output from the Varian Clinac-23EX, measured and calculated relative depth-dose data along the central-axis and dose profile at two different depths, D_{max} and 10 cm, were matched. This required some fine tuning of the incident electron beam parameters, such as its energy, energy distribution and radial intensity distribution.

A good agreement between calculated and measured dose distributions was found, except near the surface for larger fields, particularly for the 18 MV photon beam. The final primary electron beam incident on the target, to get the best fit, was found to be monoenergetic with energies of 6.4 MeV and 17.5 MeV for the 6 MV and 18 MV photon beam, respectively. The optimal radial intensity distribution of the electron beams had a Gaussian spread with widths of 1.2 mm and 1.5 mm for the 6 MV and the 18 MV photon beam, respectively. This information will be important for future treatment planning, e.g. as a benchmark for clinical treatment planning systems.

Contents

Abstract ..... *ii*

Contents ..... *iii*

1. Introduction *1*

2. Materials and methods *3*

2.1 Monte Carlo Simulations **3**
2.1.1 The accelerator and its model in BEAMnrc 3
2.1.2 Accelerator simulation with BEAMnrc 6
2.1.3 Phantom simulation with DOSXYZnrc 7

2.2 Experimental measurements **9**

2.3. Optimal values for the electron beam incident on the target **10**
2.3.1 Optimum value for the electron beam mean energy 12
2.3.2 Optimum value for the electron beam energy distribution 13
2.3.3 Optimum value for the electron beam radial intensity distribution 14
2.3.4 Investigation of the influence of the angular distribution of the primary electron beam 15

3. Results *16*

3.1 Central axis depth-dose **16**

3.2 Dose profiles **18**

3.3 Phase-space file analysis **20**

4. Discussion *21*

4.1 The component module VARMLC **21**

4.2 Electron beam parameters **22**

4.2 The discrepancy in the build-up region for high energy photon beams **23**

5. Conclusions *25*

6. Acknowledgments *26*

7. References *27*

8. Appendices *29*

8.1 Appendix 1. ..... **29**

Monte Carlo simulation with BEAMnrc/DOSXYZnrc **29**
8.1.1 ECUT and PCUT 29
8.1.2 Variance reduction 29
8.1.3 Simulation parameters in BEAMnrc 30
8.1.4 Simulation parameters in DOSXYZnrc 30
8.1.5 Time saving with variance reduction 30
8.1.5 Simulations on the cluster 31

8.2 Appendix 2. ..... **32**

Phase-space file analysis **32**

8.3 Appendix 3. ..... **38**

Investigation of the electron beam parameters **38**

9. Summary for the general public in Swedish *39*

9.1 Monte Carlo simulering av strålbehandlingsapparat – kasta tärning med fotoner **39**

1. Introduction

This project was carried out at the Radiotherapy Clinic at the Finsen Centre, Copenhagen University Hospital, Denmark. It has been preformed as a Master of Science thesis for a degree in Medical Physics at Lund University, Sweden.

Monte Carlo simulation of radiation transport is considered to be the most accurate method to calculate dose distributions. The BEAM/EGS4nrc [2] and the DOSXYZ/EGS4nrc [3] code systems are widely used Monte Carlo codes for simulating radiotherapy beams and calculating dose distributions in phantoms or in patients.

The BEAM/EGS4nrc code system is designed to simulate radiation beams from any radiotherapy source, including Co-60 and low energy x-rays. The DOSXYZ/EGS4nrc code system is designed for calculating dose distributions in rectilinear voxel geometry. Both codes are based on an electron gamma shower user code (EGS4), running under the Linux operating system.

Monte Carlo simulation can be used to obtain information about the clinical beam that cannot be measured. The knowledge of clinical beams is essential for dosimetry and for the development of accurate dose calculation algorithms in clinical treatment planning systems (TPS). Monte Carlo simulation is the most advanced and accurate technique for radiotherapy treatment planning, being based on the actual radiation transport physics. In an earlier study [16] a Monte Carlo TPS was implemented in the clinic and the dose distribution is compared with a commercial TPS. It was found that the conventional dose calculation algorithm in the commercial TPS did not accurately predict the dose distributions in and near inhomogeneities due to incorrect modelling of electron transport under charged particle dis-equilibrium. Significant differences (> 5 % in dose and > 5 mm shift in isodose lines) were found between Monte Carlo calculations and the analytical calculations implemented in the commercial systems.

The Graphical User Interface [4] (GUI) in BEAMnrc/DOSXYZnrc makes it easy for the user to use the BEAMnrc/DOSXYZnrc code without any or limited knowledge of programming.

The accelerator head geometry was built in the BEAMnrc GUI from existing component modules [1, 2] (CM), which are specifically designed to model the accelerator head. A number of scoring planes can be applied at the back plane of any CM in the accelerator where a phase-space file can be scored. The phase-space file is the most important output from BEAMnrc where information of each particle's complete history, energy, position, incident

angle and charge is stored at any specified plane in the model. The phase space file can also be used as an input file to DOSXYZnrc for further Monte Carlo dose calculations, e.g. the photon beam incident at the surface of a water phantom. In the simulations in this project a phase-space file was stored just under the accelerator head at 100 cm source-to-surface-distance (100 cm from the bremsstrahlung target).

DOSXYZnrc was used to calculate dose distributions in a water phantom. This Monte Carlo code calculates the dose in rectangular 3-D voxels when irradiated by a beam described by the output phase-space from BEAMnrc. The DOSXYZnrc has options to create a phantom by defining the properties of individual volume elements.

For the Monte Carlo calculations a state-of-the art cluster of 13 computers in a parallel architecture, each with a 2.6 MHz Intel Pentium 4 processor, was used. This reduced the calculation time when a very large number of histories were simulated.

This study aims to provide the characterization of the initial electron beam as it leaves the accelerator vacuum and hits the bremsstrahlung target. This feature requires some fine tuning of different parameters for the electron beam in order to match Monte Carlo calculated dose distributions with measured dose distributions into satisfactory agreement. This study will also give more comprehensive information for radiotherapy photon beams, such as the mean energy of incident photons and electrons and their angular distributions. This is presented in Appendix 2.

2. Materials and methods

2.1 Monte Carlo Simulations

2.1.1 The accelerator and its model in BEAMnrc

Two photon beams from a Varian Clinac-EX23 linear accelerator (*Varian Medical Systems, Palo Alto, CA, USA*) at Finsen Centre, Copenhagen University Hospital Denmark were simulated. The accelerator was installed at the clinic in the beginning of 2002. The multi-leaf collimator (MLC) system is a Varian Millennium 120 leaf MLC, with 80 inner leaves and 40 outer leaves with a projected width at isocentre of 0.5 cm and 1.0 cm, respectively. All the dimensions and the material for the accelerator head were incorporated according to the manufacture's detailed specifications.

The geometry of the accelerator, i.e. all of the essential components in the treatment head, was built in BEAMnrc using a number of individual component modules (CM) that is perpendicular to the beam axis. There are predefined component modules in BEAMnrc which are useful for different components in the treatment head. It is possible to modify the CM, the physical dimensions and material, to match the specific components according to the manufacturer's specification. Since some CMs are used for many different components in the accelerator head each CM was given a unique name so that a particular CM could be used more than once, e.g. *target* for the CM SLABS when it was used for the bremsstrahlung target.

The CMs used in this study to model the Varian Clinac-23EX were: SLABS for target, CONS3R for primary collimators, SLABS for vacuum window, FLATFILT for flattening filter, CHAMBER for ionising chamber, MIRROR for mirror, JAWS for secondary collimators (X1, X2, Y1 and Y2), VARMLC for MLC, SLABS for exit window and SLABS for the air gap between the exit window and the phantom surface at SSD = 100 cm. An illustration of the accelerator and all its modelled components can bee seen in Figure 1.

The accelerator module must be compiled before it can be used.

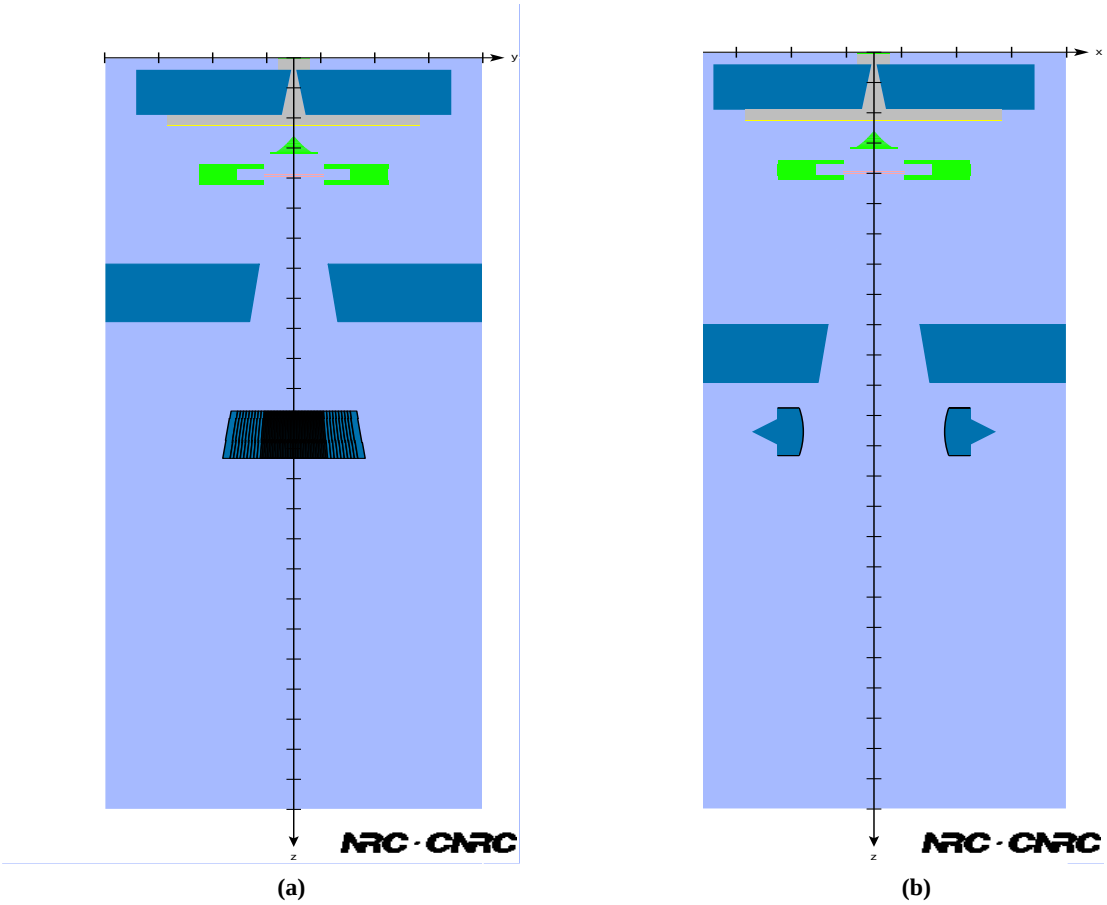

(a) (b)

Figure 1. Illustration (not to scale) of the accelerator (6 MV) and the different component modules in (a) xz-plane and (b) yz-plane.

In clinical linear accelerators (linacs) a conical beam-flattening filter is used for photon beams since the intensity of photons is peaked in the forward direction. Such a filter attenuates the photon beam more strongly in the central parts. The exact alignment of the filter is of course critical. With the component module FLATFILT [2], for modelling the flattening filter, the user can specify the flattening filter geometry exactly according to the manufacturer's detailed specifications.

For the 6 MV photon beam, the Compton effect is the most important interaction mechanism ss the filter is made out of a lower-Z material (Z around 30). The approximate shape of the filter can be seen in Figure 2b. This filter attenuates the beam more strongly in the central part and mainly removes low energy photons below a few hundred keV through photoelectric effect without changing the spectral shape of the higher energies.

For the 18 MV photon beam, pair production becomes important. The use of a thick high-Z filter in a high megavoltage x-ray beam tends to filter out the high-energy photons through pair production as well as the low-energy photons through photoelectric effect. The 18 MV flattening filter has an inner cone made of a high-Z material to achieve more uniform energy fluence through the field. The outer and the bottom part of the filter are made of a lower-Z material. The approximate shape of the filter can bee seen in Figure 2a.

(a) **(b)**

Figure 2. Illustration (not to scale) of CM FLATFLT for the flattening filter for the (a) 18 MV and (b) 6MV photon beam

In BEAMnrc [2] there is unfortunately no CM to model the exact geometry of the new Varian Millennium 120 MLC. With the CM used in this study, the VARMLC [2], it is, however, possible to specify some of the physical properties of the MLC such as; the individual leaf thickness, the tongue and groove width and length, the rounded leaf ends and the air gap between the leaves. The leaf sides can be focused at z = 0 (i.e. the sides of the MLC leaves are focused towards the target). However this is not enough to specify the exact details of the Varian Millennium 120 MLC leaf. There are leaf tips, driving screw holes (which is a 3 mm slit in the leaf to allow travel of the lead screw) and supporting rail grooves which cannot be specified in VARMLC.

Since the modelling of the supporting rail groove and the leaf tip is not supported by the simplified model (VARMLC), the inner and outer leaf thickness are reduced with approximately 3.5% and 6 %, respectively [12] to compensate for the missing material. The upper edge of the MLC, ZMIN, was specified to be 47 cm from the target, the interleaf air gap was set to 0.006 cm and the thickness of the inner and outer leaves was set to 0.229 cm and 0.464 cm respectively, at ZMIN.

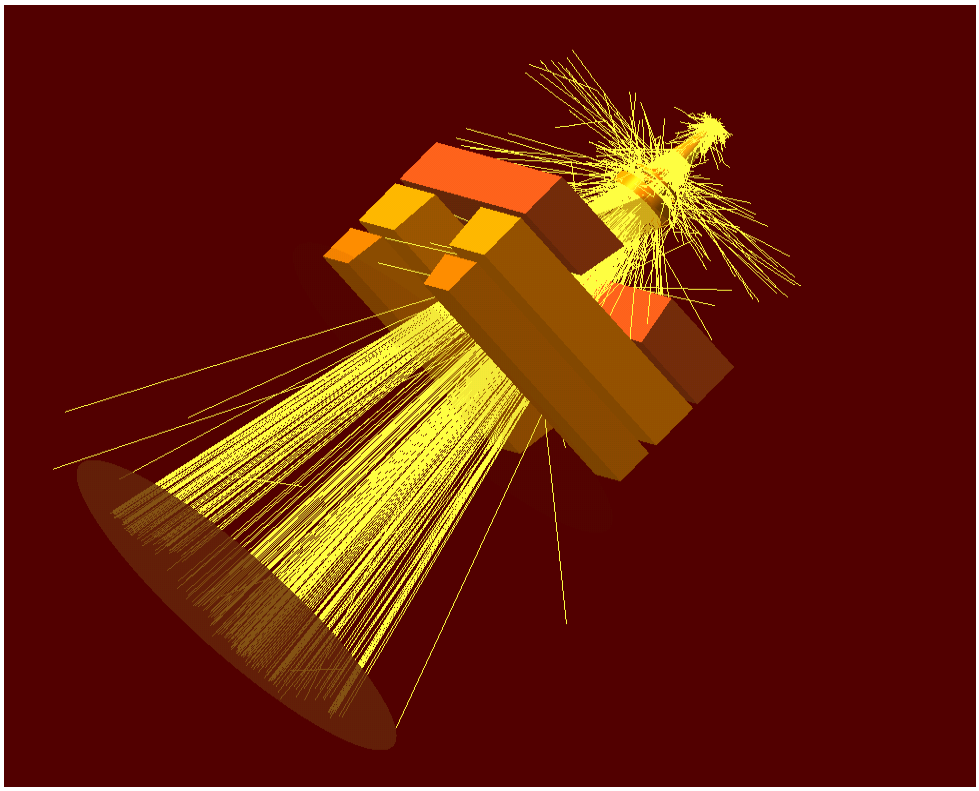

Figure 3. Illustration of the accelerator in EGS_windows_4.0 [5]. EGS_windows_4.0 is a 3-D tool for interactively display the geometry of the accelerator and the track history for all different particles (photons, electrons and positrons).

2.1.2 Accelerator simulation with BEAMnrc

An inherent problem in Linux is that the system cannot handle file lengths greater than roughly 2 Gbyte. As a consequence, there is an upper limit for the number of histories that can be stored in the phase-space file. A phase-space file was collected at SSD = 100 cm for each simulation.

The total number of histories simulated was dependent on each situation. Since the radiation yield, $Y(T_0)$, for tungsten is approximately twice as large for the 18 MV beam as for the 6 MV beam, fewer electrons incident on the target were needed for the 18 MV beam.

The CPU time, when all the nodes of the cluster was being used, was 1.5 hours for the 18 MV photon beam and the larger field (40 x 40 cm^2), running approximately 100.000 histories per hour. The CPU time (with all the 13 nodes being used) for the 6 MV photon beam was 1 hour running approximately 1.4 million histories per hour for the larger field. These simulations gave approximately a maximum of 67 million histories in the phase-space file.

For details about simulation parameters, see Appendix 1.

2.1.3 Phantom simulation with DOSXYZnrc

To obtain the most accurate simulation the size of the simulated phantom matched the size of the phantom used for the experimental measurements. The volume surrounding the water phantom was set to air, and the phase-space file from BEAMnrc was used as input file for the beam. The number of histories required in each run to get a desired statistical uncertainty is dependent on the field size, voxel size and the photon energy. In areas where the dose gradients were large, smaller voxels were necessary and therefore a larger number of histories was required to get the desired statistical uncertainty. The number of particles for each beam was set to obtain less than 1 % statistical uncertainty (1 S.D.) in the smallest voxels of each simulation.

To calculate the approximate number of histories needed at the phantom surface in order to obtain a desired statistical uncertainty in each voxel, the following formula [18] was used:

$$N = \frac{1}{\delta^2 \mu_{en}^{eff}} \frac{A_{beam}}{V_{voxel}} \qquad (1)$$

where N is the total number of histories at the phantom surface, A_{beam} is the field size, δ is the statistical uncertainty (e.g. 0.01 to achieve 1 S.D. equal to 1 %) desired in the simulations, μ_{en}^{eff} is the effective energy absorption coefficient in water for photons and V_{voxel} is the volume of the voxels where dose is calculated.

When phase-space data is sparse or insufficient, the particles can be re-used to improve the statistics in the dose calculations. Each time a particle is re-used it will get a new unique pair of seeds (numbers) to generate a random number sequence. In order to reduce the systematic uncertainties due to small data set, DOSXYZnrc can redistribute the particles, as long as the simulated linac geometry is symmetric, and the treatment field is centred on the beam-axis.

Nevertheless, recycling has consequences when for example the particle fluence is insufficient in the phase-space file. If the statistics in the phase-space is good enough to represent all classes (e.g. photons vs. electrons, or scatter vs. direct) of particles, the phase-space can be recycled up to 80-90 times [7]. It has also been shown that recycling of histories has an effect on the uncertainties in dose calculation [24]. This effect is not as dramatic when recycling a photon source as when recycling an electron source since the photons are less likely to interact in the same voxel.

Since the maximum size of the phase-space file is 2048 megabyte, the data in the phase-space files was insufficient, and had to be reused in all simulations.

The size of the scoring voxels during the DOSXYZnrc simulation varied between 1.0 x 1.0 x 0.2 cm^3 (xyz) and 4.0 x 4.0 x 1.0 cm^3 for the depth-dose calculations along the central axis and between 0.2 x 2.0 x 0.5 cm^3 and 1.0 x 3.0 x 0.5 cm^3 for the profile calculations, depending on the spatial resolution required. In the penumbra region and the build-up region, the smaller voxel size was chosen. The scoring voxels for the profiles were centred at 1.5 cm and at 3 cm depth for the 6 MV and 18 MV beams, respectively, and at a depth of 10 cm.

The total number of histories simulated was dependent on each situation. The number of particles generated by the phase-space file were for example in the order of 3 x 10^9 for a 6 MV photon beam, 40 x 40 cm^2 field size, for the profile calculations.

The typical CPU time (on each node of the cluster) was 5 hours, simulating approximately 45 million histories per hour. For details about simulation parameters, see Appendix 1.

2.2 Experimental measurements

The measurements were performed on linear accelerator number 9, a Varian Clinac-23EX, at the radiotherapy clinic at the Finsen Centre, Copenhagen University Hospital in Denmark.
All the measurements were made using a Scanditronix-Wellhöfer RFA-300 scanner and a RK-8305 ionisation chamber. The scanning volume and the servo range of the water phantom have the dimensions 495 x 495 x 495 mm^3. The scanning system has a position accuracy of ± 0.5 mm and a reproducibility of ± 0.1 mm. The RK-chamber is a cylindrical ionisations chamber with an inner cavity volume of 0.12 cm^3 (r = 2 mm). The effective point of measurement for the ion chamber was taken to be 0.75*r up-streams. All measurements were made in water. A reference chamber was placed in the field to correct for beam output variations during scanning.
The software OmniPro Accept 6.1 (Scanditonix-Wellhöfer) was used for data collection. The parameters set for the profile scans were: medium speed, precision mode, small step size 1 mm, large step size 2 mm and delta dose 1 % and the parameters set for the depth-dose scans were: low speed, precision mode, small step size 2 mm, large step size 3 mm and delta dose 3 %. Delta dose is the percentage change in dose between two measuring points.

Figure 4. Machine nr 9, a Varian Clinac-23EX, at the radiotherapy clinic at the Finsen Centre, Copenhagen University Hospital in Denmark and the Scanditronix-Wellhöfer RFA-300 beam scanner.

2.3. Optimal values for the electron beam incident on the target

One way to describe the characteristics of a clinical photon beam is to measure depth-dose curves and profiles. By validating Monte Carlo calculated dose distributions with experimental measured dose distributions, an electron beam can be derived that will, when it hits the bremsstrahlung target in the treatment head, produce a photon beam that has the same characteristics as the clinical photon beam.

The depth-dose curves are sensitive to the electron beam energy and its energy distribution, but they show no significant sensitivity to the radial intensity distribution [6, 9]. The so-called "horns" on the profiles are, however, found to be very sensitive to any change in the radial intensity distribution of the electron beam as it hits the target.

The stopping-power ratio varies slightly with depth and in some other studies [6, 9, 10] these variations have been taken into account. For larger fields the stopping-power ratio varies less than for smaller fields [6, 9]. The variation in stopping-power with depth, for a 10 x 10 cm^2 field, is about 0.5 % at 6 MV and 1 % at 18 MV, from the surface to 40 cm depth in water [9]. However from D_{max} to the depth of 30 cm, the variation is only about 0.2 % at 6 MV and about 0.3 % at 18 MV for the smaller field, 10 x 10 cm^2. For the larger field, 40 x 40 cm^2, the variation between these depths is less than about 0.1 % for both energies. For this reason the variation of the stopping-power ratio was not considered in this study and the largest field size, 40 x 40 cm^2, was used when matching the depth-dose curves.

In this project depth-dose curves along the central axis and profiles at two depths, D_{max} and 10 cm, were simulated for different settings of four separate electron beam parameters: mean energy, energy distribution, radial intensity and angular distribution. There are several different beam source routines available in BEAMnrc and three of them were used in this project. When comparing the simulations with the measurements, all data were normalized at 10 cm depth.

The procedure to find the correct initial electron beam is described by the flowchart in Figure 5. Other parameters, such as densities of the target and flattening filters and the detailed geometry of the latter were not investigated, as it was assumed that the material specifications provided by the manufacturer were accurate.

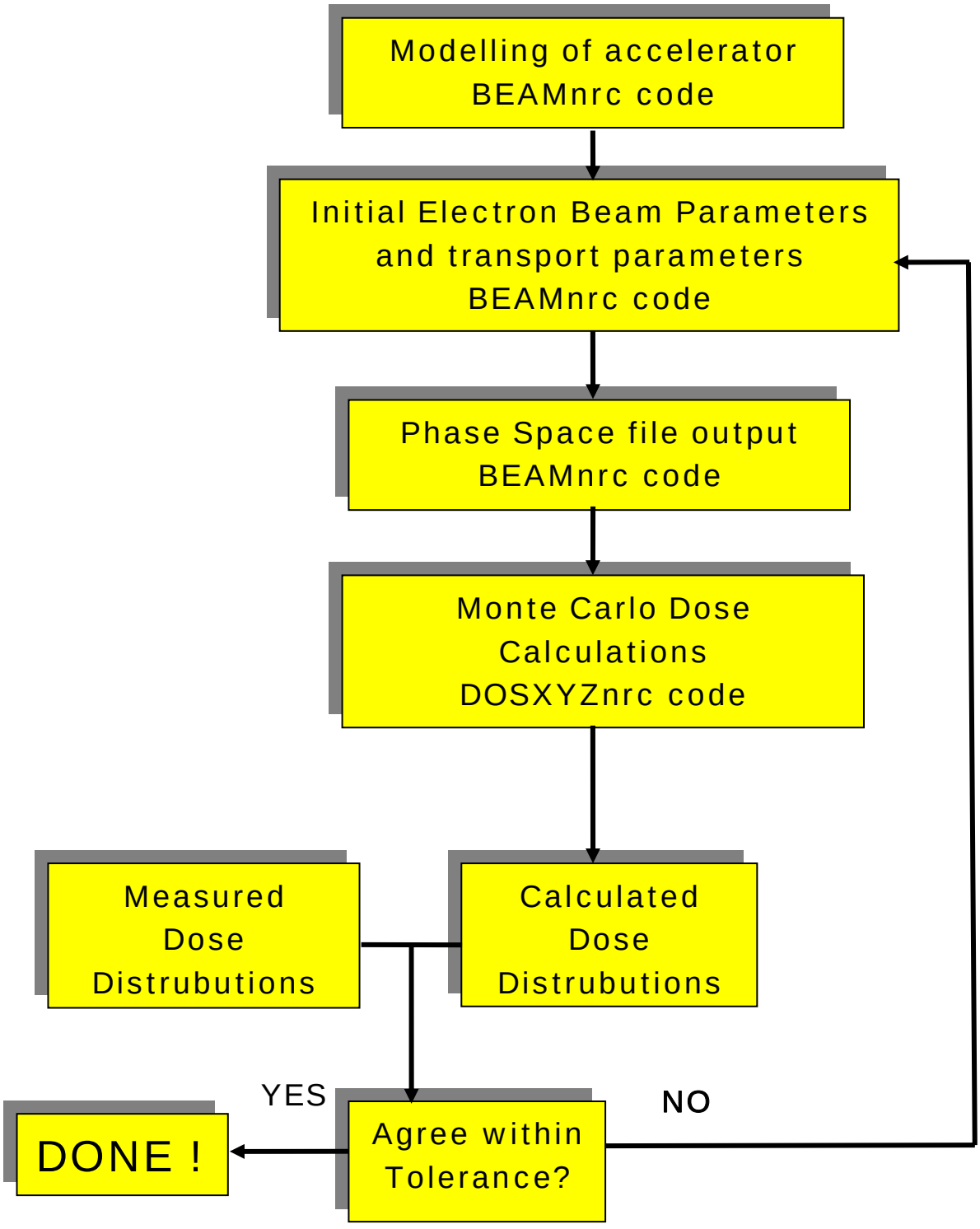

Figure 5. Flowchart of the procedure on how to find the accurate description of the incident electron beam at the target

2.3.1 Optimum value for the electron beam mean energy

When fast electrons interact in matter, part of their energy is converted into electromagnetic radiation in the form of bremsstrahlung. The rate of bremsstrahlung production by electrons is expressed by the *mass radiative stopping power* ($dT/(\rho \cdot dx)$) and it increases with increasing electron energy. The fluence of bremsstrahlung photons in the forward direction increase with energy more strongly than does the fluence of bremsstrahlung photons in other directions. At $\theta = 0^\circ$ the x-ray energy fluence tends to increase as T_0^4 for $T_0 \approx 1$ MeV, as $T_0^{2.3}$ at $\approx$ 10 MeV and as T_0^2 at $\approx$ 100 MeV [21], where T_0 is the mean energy of the electron beam. Since the intensity of photons in the forward direction increases with energy, the relative intensity between the forward direction and other directions increase with energy. This leads to a decrease of the horns on the bremsstrahlung energy fluence profile with increasing energy of the primary electron beam incident on the target.

The mass scattering power of electrons decreases with energy. This implies that the electron scatter less before the production of bremsstrahlung photons as the electron energy increases. The angular distribution of the produced high-energy photons is narrowed.

These two factors, the intensity of photons created in the forward direction and electron scatter will influence the shape of the dose-profiles as the mean energy is changed.

The source routine ISOURC =1 (see Figure 7b), which is a parallel circular beam with a uniform radial intensity distribution along the central axis, was used to find the suitable mean energy by varying it in steps of 0.1 MeV. The depth-dose curve along the central axis was found to be quite insensitive to small changes of energy ($\pm$ 0.2 MeV). However, the shape of the profiles were changed even for smaller changes in energy ($\pm$ 0.1 MeV), yielding increasing horns with decreasing energy. Since the depth-dose curve was not as energy dependent, the shape of the profiles was more important while tuning the energy. For results, see Appendix 3.

2.3.2 Optimum value for the electron beam energy distribution

The primary electrons will have a certain energy distribution when leaving the wave guide of the accelerator. In clinical linacs, such as the one studied here, the accelerator tube is often too long to be placed vertical in the treatment head. This means that the electron beam has to be bent to hit the bremsstrahlung target in the treatment head. The precision of the electron beam bending is accomplished by the beam transport system consisting of bending magnets, focusing coils and other components. In a Varian Clinac-23EX the angle between the accelerator tube and the target is 90 degrees and an achromatic 270 degree bending magnet is used (see Figure 5). Since the electrons are not perfectly mono energetic they will not travel in the same orbit through the bending magnet. By placing an energy slit in the bending magnet orbit an energy selection can be made (see Figure 5a). The energy distribution of the electron beam is dependent on the width of the slit and the field strength of the bending magnet.

Different Gaussian distributions were investigated in this study to describe the energy distribution of the primary electron beam incident on the target. Since the profiles were very sensitive to the mean energy one might expect the energy distribution to be important as well. However, in this study it did not show any significant importance. The depth-dose curve showed no sensitivity to the energy distribution and the effects on the profiles were hardly detectible. But it is still not realistic to believe that the electron beam is monoenergetic. According to the manufacture, the energy slit will restrict the energy spread to ± 3 %.

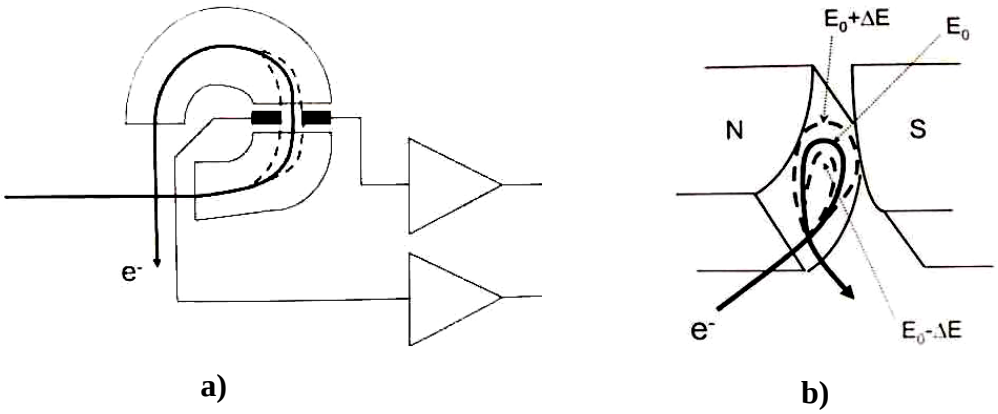

Figure 6. These are simplified illustrations of a) the energy slit and b) the achromatic 270 degree bending magnet with its energy distribution.

2.3.3 Optimum value for the electron beam radial intensity distribution

The primary electron beam has a radial intensity distribution and an angular distribution after the 270 degree achromatic bending magnet when it hits the bremsstrahlung target.

In this study two different radial intensity distributions were investigated. The two source routines used were: parallel circular beam from the front with a uniform intensity distribution (ISOURC = 1, see Figure 7b) and a parallel circular beam with a 2-D Gaussian intensity distribution (ISOURC = 19, see Figure 7a). Various sizes of radii and different FWHM's of the Gaussian radial intensity distributions were investigated in steps of 0.2 cm. The horns of the profile were found to be dependant to the intensity distribution, the size of FWHM or the size of the radii. On the other hand, the profiles did not show any significant differences between the uniform and Gaussian beam intensity. For results, see Appendix 3. The intensity distribution showed no effect on the depth-dose curve along the central axis.

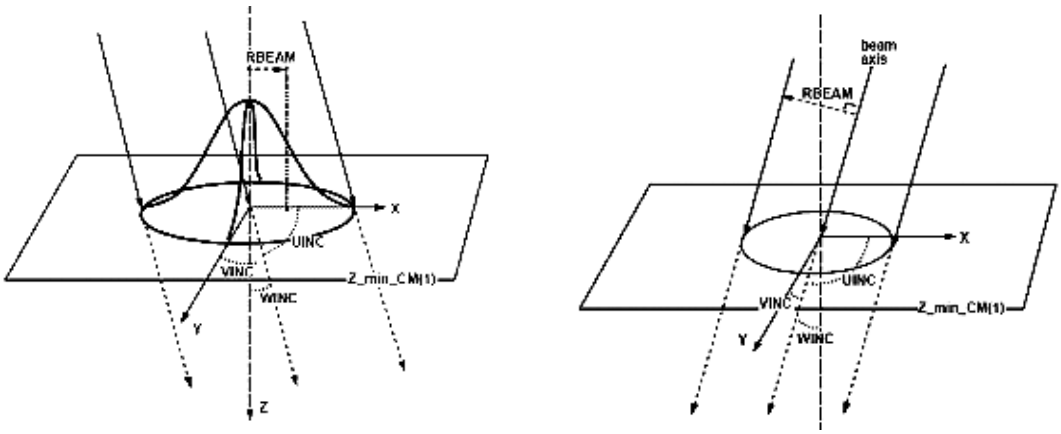

a) **b)**

Figure 7. The geometry of a) Parallel Circular Beam with 2-D Gaussian XY- Distribution (ISOURC = 19) [2] and b) Parallel circular beam with a uniform distribution (ISOURC = 1) [2]

2.3.4 Investigation of the influence of the angular distribution of the primary electron beam

It is most likely that the primary electron beam incident on the target is not a perfect parallel beam but that the electrons will have an angular distribution when they hit the target. There is not any specific source routine in BEAMnrc describing an electron source having an angular distribution. Consequently, in order to investigate the influence of the angle distribution of the electron beam a parallel beam that is swept around an imaginary cone was used.

In a study, which concerned the NRC linac [6] (National Research Council Canada), it is shown that the sweeping angle has a considerable effect on the entire shape of the profile. The linac in this particular study [6] had an electron beam which was scanned on the surface of a cone with a measured half-angle of $4.2^\circ \pm 0.3^\circ$ to obtain flatness. Changing simulated angle by 0.1° made the shoulder region of the profiles 3 % higher at D_{max}.

The source routine used was the NRC swept beam ISOURC = 5 (se Figure 8) which is a parallel circular beam swept around the outside of an imaginary cone where GAMMA is the half-angle of the cone in degrees and RBEAM is the beam radius in cm. This source routine was considered to be a good approximation for a source with an angular distribution.

The horns of the profile were very sensitive to the angle of the cone. The intensity of the fluence increases in the periphery of the beam, as the angle increases, and as expected a larger angle results in larger horns. For results, see Appendix 3.

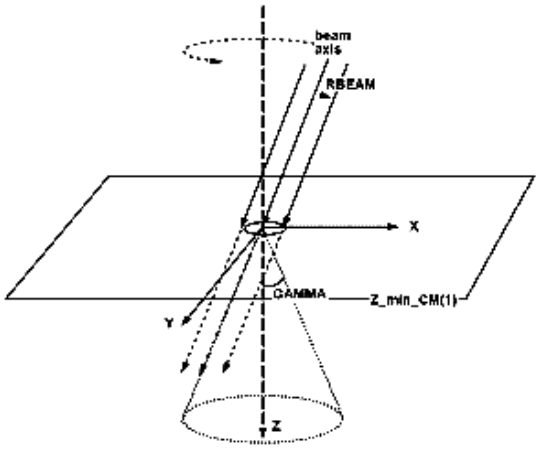

Figure 8. The geometry of the NRC swept beam source (ISOURC = 5) [2]

3. Results

Data from Monte Carlo calculations was compared with the experimental measured data. A combination of the free parameters; mean energy, energy distribution, radial intensity distribution and angular distribution of the primary electron beam were investigated and an electron beam was found for the best fit. This primary electron beam was monoenergetic with energies 6.4 MeV and 17.5 MeV and the radial spread was Gaussian with FWHM sizes of 1.2 mm and 1.5 mm for the 6 MV and the 18 MV, respectively.

Figure 9-12 presents a detailed comparison of the depth-dose curves, showing an agreement within 1 % (local dose), except at shallower depths for larger fields and for the dose in the build-up region for 18 MV and larger fields. This is a well-known problem [7, 9, 11, 22, 23] which is discussed in section 4.2. Figures 13-16 presents a detailed comparison of the profiles, showing an agreement within 2 % (local dose), except at D_{max} for the 18 MV photon beam.

3.1 Central axis depth-dose

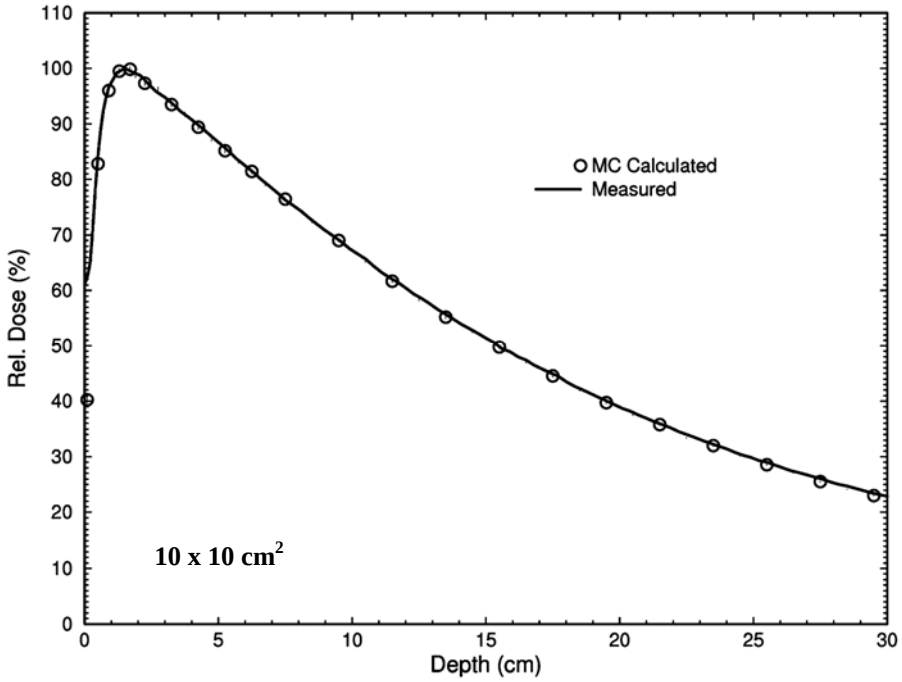

Figure 9. The 6 MV photon depth-dose curve in water for 10 x 10 cm^2 field at 100 cm SSD. MC denotes the data from Monte Carlo calculations.

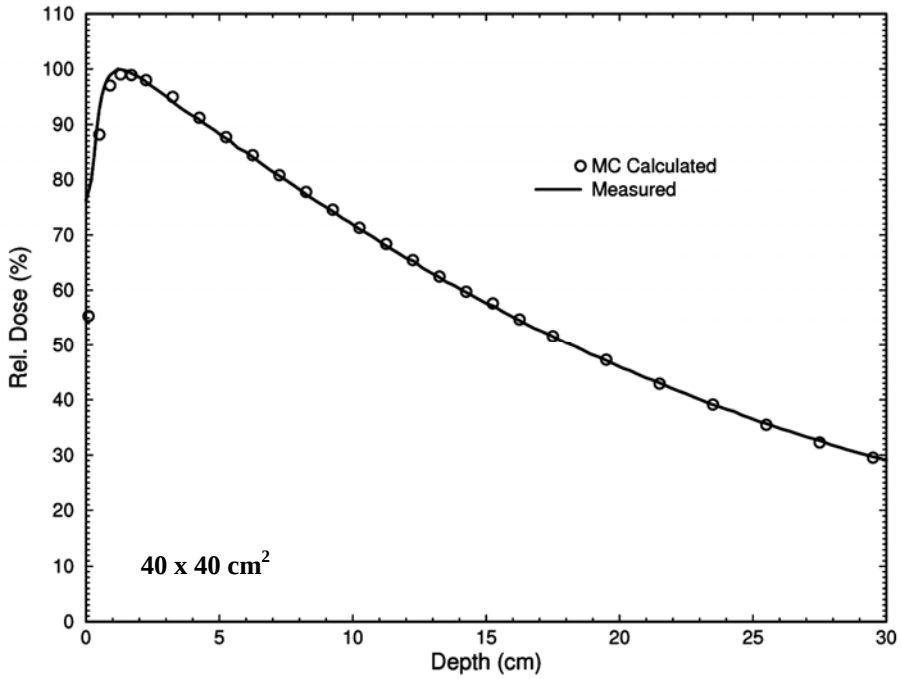

Figure 10. The 6 MV photon depth-dose curve for 40 x 40 cm^2 field at 100 cm SSD. MC denotes the data from Monte Carlo calculations.

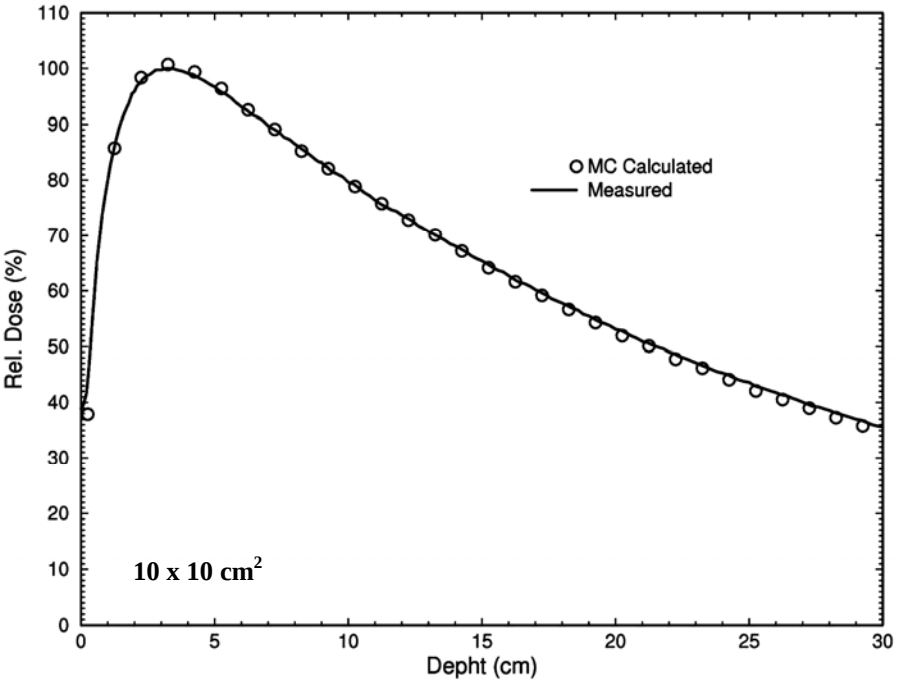

Figure 11. The 18 MV photon depth-dose curve in water for 10 x 10 cm^2 field at 100 cm SSD. MC denotes the data from Monte Carlo calculations.

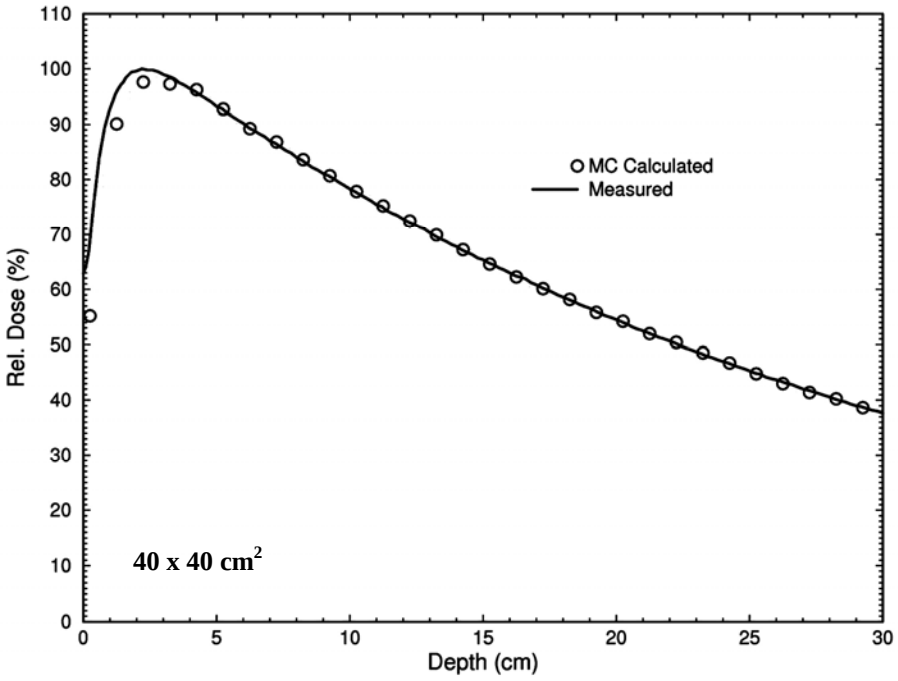

Figure 12. The 18 MV photon depth-dose curve in water for 40 x 40 cm^2 field at 100 cm SSD. MC denotes the data from Monte Carlo calculations. There are large discrepancies in the build-up area.

3.2 Dose profiles

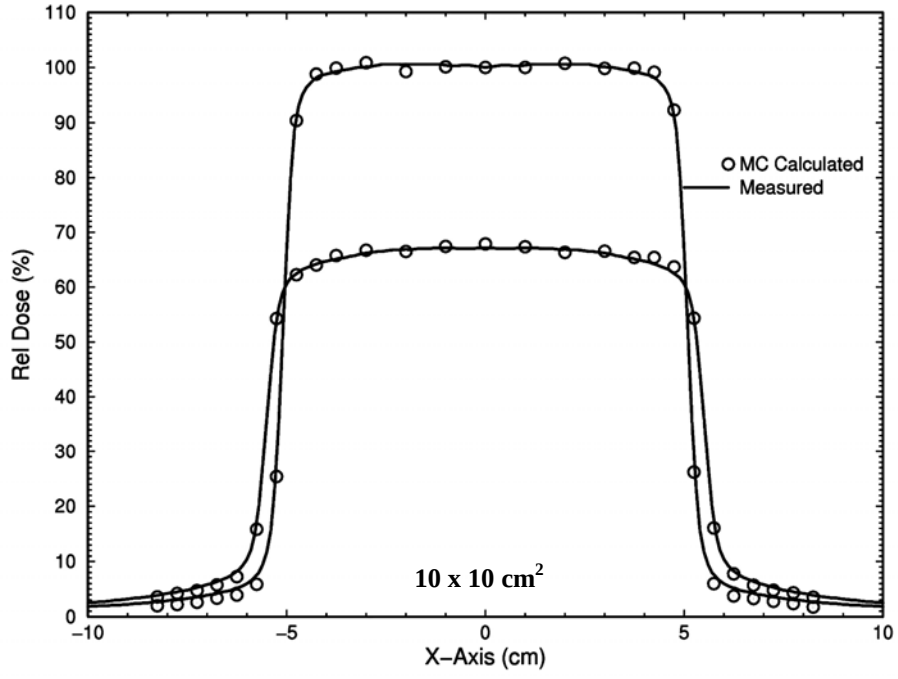

Figure 13. The 6 MV photon beam profile in water for a 10 x 10 cm^2 field at 1.5 and 10 cm depths. The profiles are presented along the X-jaws.

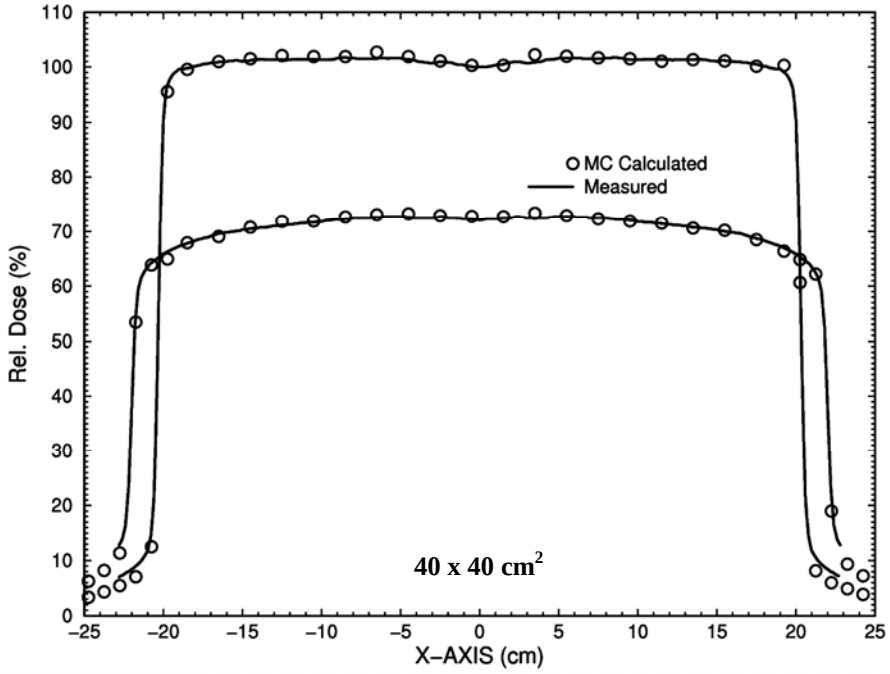

Figure 14. The 6 MV photon beam profile in water for a 40 x 40 cm^2 field at 1.5 and 10 cm depths. The profiles are presented along the X-jaws.

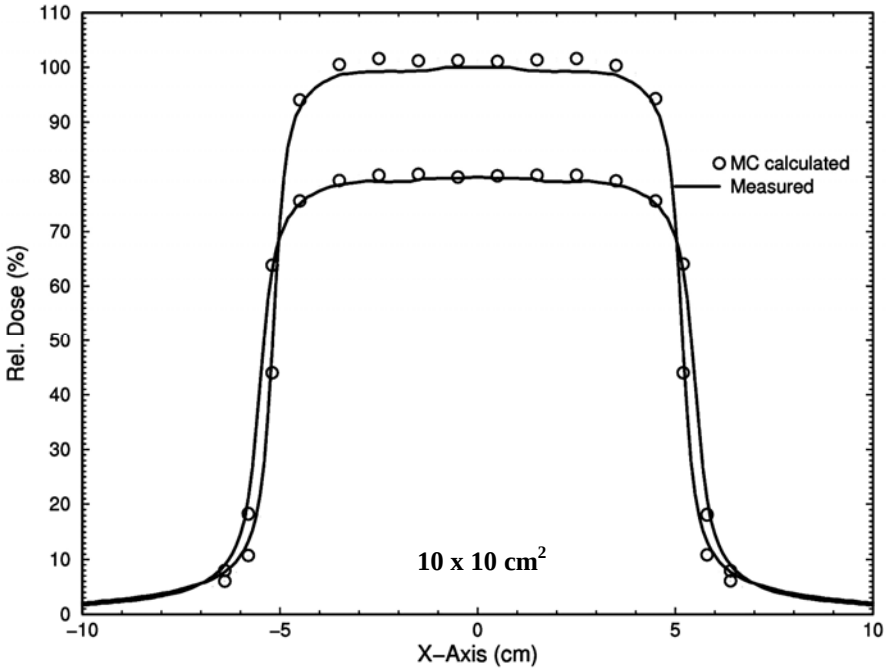

Figure 15. The 18 MV photon beam profile in water for a 10 x 10 cm^2 field at 1.5 and 10 cm depths. The profiles are presented along the X-jaws.

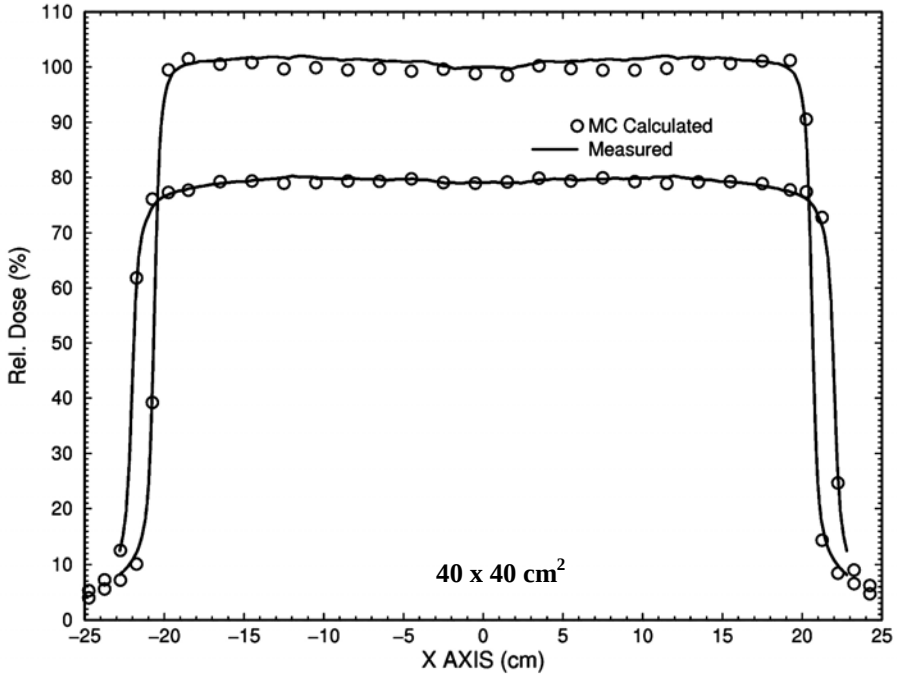

Figure 16. The 18 MV photon beam profile in water for a 40 x 40 cm^2 field at 1.5 and 10 cm depths. The profiles are presented along the X-jaws. The profiles are match on the depth of 10 cm, since there are large discrepancies in the build-up area.

Since there were problems with discrepancies in the build-up area for the larger fields at 18 MV, the profiles were matched at the depth of 10 cm for the larger field, in order to get the best agreement between the calculations and the measurements. When the best match was found for the larger field at 18 MV, the match for the smaller field was unfortunately not satisfactory. This needs further investigation.

3.3 Phase-space file analysis

The phase-space files scored at the phantom surface at SSD = 100 cm were investigated with the BEAMnrc data processor, BEAMDP. Energy spectra, fluence profiles, energy fluence profiles, mean energy profiles and angular distributions at the phantom surface are presented in Appendix 2.

4. Discussion

4.1 The component module VARMLC

Heath and Seuntjens [12] developed a new component module, the DYNVMLC [12], to fully model the geometry of the Varian Millennium 120 MLC, and the DYNVMLC (Figure 17b) and VARMLC (Figure 17a) were compared with respect to, among other parameters, interleaf leakage. They [12] concluded that the differences found in dose distributions may not appear significant for a single field but in treatments where multiple fields are used, like in IMRT, the summed differences may be significant in the low dose regions as VARMLC underestimates the leaf transmission.

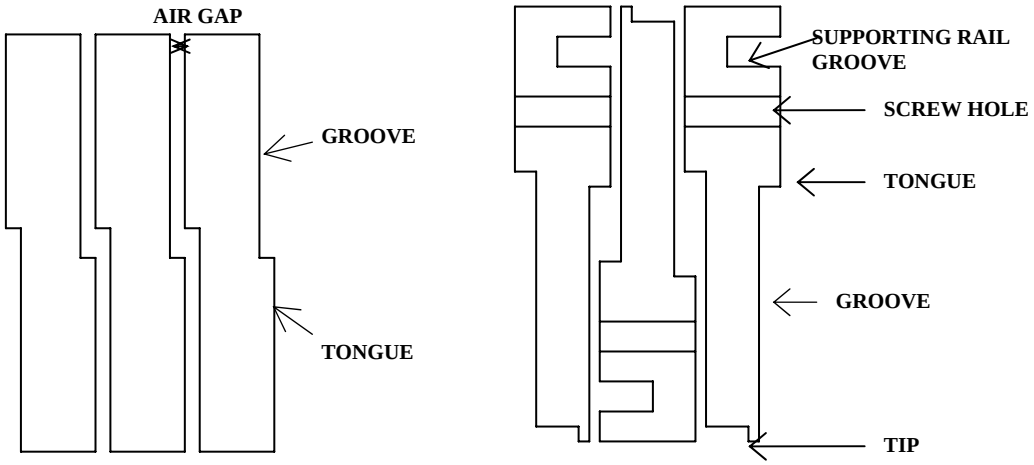

Figure 17. A simplified illustration of the component module (a) VARMLC and (b) DYNVMLC

Other attempts have been made to develop new component modules in BEAMnrc to get a more accurate description of the different kinds of multi-leaf collimators (MLC). De Walle et al. [13] developed a CM called MLCE to fully model the Elekta MLC, where interleaf leakage and transmission through the leaves were investigated.

If the intrinsic electron beam data found in this study are going to be used in treatment planning where the MLC is required, a new CM for the Varian Millennium 120 MLC needs to be developed. Especially since the dose in low-dose areas is overestimated using the VARMLC [12].

4.2 Electron beam parameters

Over the years, much effort has been devoted to Monte Carlo simulations of different accelerators. A comparison of the derived parameters from previous publications concerning Monte Carlo modelling of Varian accelerators and this work is listed in the Table 1 below. Sheikh-Bagheri and Rogers [7] have probably performed the most comprehensive study and they concluded that the two most important parameters for simulating photon beams is the mean energy and the radial intensity distribution of the incident electron beam.

Table 1. A comparison of the result in this work with other studies that have used Monte Carlo methods to model Varian accelerators.

Author	Accelerator	Nominal Energy (MV)	Mean electron energy (MeV)	FWHM energy spread (% of mean)	Electron radial distribution	Depth-dose agreement with measurements
Sheikh-Bagheri and Rogers [7]	Clinac High energy	6	5.7	3 %	2.0 mm FWHM Gaussian function	Good
Sheikh-Bagheri and Rogers [7]	Clinac High energy	18	18.3	3 %	1.1 mm FWHM Gaussian function	Calculated dose to low in the build-up
Ding [9]	2100EX	6	6.02	17 %	1.2 mm FWHM Gaussian function	Good
Ding [9]	2100EX	18	18	6 %	1.5 mm FWHM Gaussian function	Calculated dose low in build-up for larger fields
S. H. Cho *et al.* [11]	2100 series	6	6.2	3 %	1.0 mm FWHM Gaussian function	Relatively poor for larger fields in the build-up. Good for smaller fields.
P. J. Keall *et al*. [22]	2100EX	6	6.2	3 %	1.3 mm FWHM Gaussian function	Good
P. J. Keall *et al*. [22]	2100EX	18	17.0	3%	1.4 mm FWHM Gaussian function	Calculated dose low for shallow depth
Hartmann-Siantar *et al*. [23]	Clinac High energy	6	6.2	0	2 mm diameter cylindrical function	Good
Hartmann-Siantar *et al*. [23]	Clinac High energy	18	18.5	0	2 mm diameter cylindrical function	Calculated dose low in build-up region for larger fields
This work	23EX	6	6.4	0	1.2 mm FWHM Gaussian function	Good, except for shallow depth at larger fields
This work	23EX	18	17.4	0	1.5 mm FWHM Gaussian function	Calculated dose low in build-up region at larger fields

The depth-dose curves in this study were not as sensitive in changes to the incident electron beam parameters as were the profiles. The horns on the profiles were very susceptible to the mean energy, the width of the primary electron beam and as well as to the incident angle distribution of the beam. By merely adjusting these three parameters, the whole shape of the simulated profile could be manipulated to get a good agreement with the measured profiles.
The simulations could have been done with a primary electron beam with an energy spread of ± 3 %, but it was not used in this study since it did not have any significant consequence on either the depth-dose curves or the dose profiles.

4.2 The discrepancy in the build-up region for high energy photon beams

The discrepancy in the build-up region for high energy photon beams is a well known problem [7, 9, 11, 22, 23]. Ding [9] simulated 6 and 18 MV photon beams from a Varian 2100EX and encountered problems with matching of dose distributions for the 18 MV at 40 x 40 cm^2 field in the build-up region. It appears that something present in high-energy photon beams, but not modelled in the EGS calculations, was responsible. One suggestion was that it possibly could be caused by neutron activation, but a further investigation [20] came to the conclusion that the neutrons are unlikely to be responsible since the IC-10 chamber used is not highly sensitive to neutrons.
In 18 MV photon beams most of the contaminating electrons originate from components in the treatment head, while most of the these electrons in a 6 MV photon beam originate from the air gap between the accelerator head and the phantom and from the air in the head itself. One reason for the difference in the 18 MV beam could be that there is some part of the treatment head that generates contaminant electrons which is missing in the simulation. To derive the effect of these missing contaminating electrons, the treatment head geometry was investigated in order to find some component that was close enough to the beam and that could have an influence. Close to the mirror in the treatment head there is a lot of shielding material made of tungsten and lead and this shielding relatively close to the photon beams. Simulations for the 18 MV photon beam 40 x 40 cm^2 field were done, where the shielding material surrounding the mirror was included, to investigate if the contaminant electron fluence at the phantom surface increased.

The electron spectra and the energy fluence at the phantom surface were analyzed using the auxiliary part of BEAMnrc, BEAMDP. The result showed an increase of low energy electrons and an increase in over all energy fluence (se Figure 18). This however, was not enough to fully account the discrepancy in the build-up region.

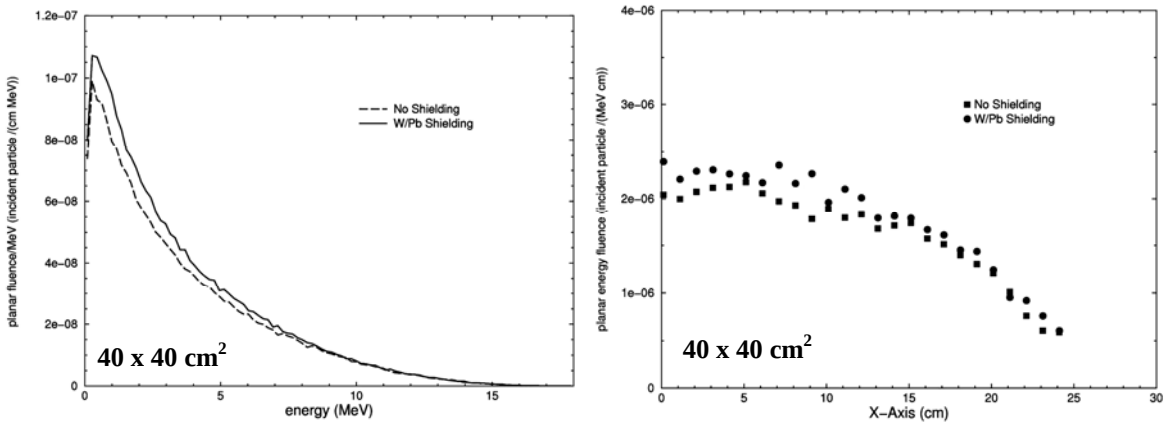

Figure 18. Electron spectra and energy fluence vs. position for electrons for an 18 MV photon beam at the surface of a water phantom at SSD = 100 cm

This inability to accurately model high-energy photon beams may depend on many different factors, such as densities of the components used and the detailed geometry of the flattening filter specified by the manufacturer. For instance, the specifications from the manufacturer that were used in this study are more than eight years old. Since the accelerator models are constantly improving, should there not be some changes to the specifications? Is it possible that nothing has been changed in Varian's accelerators over all these years? The model Clinac-23EX did not even exist eight years ago.

Other factors that could influence the inability to correctly model high-energy photon beams could be due to shortcomings in the cross sections, or transport methods used by the Monte Carlo code, or the conversion from measured ionization to dose are incorrect.

5. Conclusions

This study presents the characterisation of 6 and 18 MV photon beams from a Varian Clinac-23EX accelerator for field sizes of 10 x 10 cm^2 and 40 x 40 cm^2. The characterisation of the photon beams was based on Monte Carlo simulations using the EGS4 user codes BEAMnrc and DOSXYZnrc. To estimate the incident electron beam energy and radial intensity distribution, profiles and depth-dose curves were compared with experimental measurements. Detailed information of the beam characteristics is very useful for future development of treatment planning systems.

The calculated and measured dose distributions in the water phantom were in excellent agreement in all cases except for the 18 MV photon beam at the larger field size, 40 x 40 cm^2, in the build-up region. The cause of this discrepancy needs further investigation.

6. Acknowledgments

First of all I would like to thank my excellent supervisors Lasse Rye Aarup and Håkan Nyström for their guidance and engagement through this work.
Lasse, thanks for helping me out with BEAMnrc and DOSXYZnrc and giving me a basic understanding of the operating system Linux. Am I a nerdess yet?
Håkan, thanks for all your ideas in how to solve problems and for all your expertise help with the physics.

I was fortunate to have the opportunity to discuss some simulation issues in BEAM/DOSXYZ with Tommy Knöös at the Radiation Physics Department at the University Hospital in Lund, Sweden. Thank you!

I also would like to thank Sofie Månsson for helping me out with the experimental measurements and for making me feel at home at the clinic from the first day. Thanks for being a superb roommate and for your endless positive thinking.

Per Engström, I would like to thank you for your proof-reading and the fact that you endured all the female giggling in our office. Thanks!

Thanks to Chand and Wendy Sapru for your proof-reading.

During the writing of this thesis I've been supported by many different people at the radiotherapy clinic at Finsen Centre at the University Hospital in Copenhagen, Denmark. Your help has been in many different ways and I would like to thank you all!

A special thanks goes to my mother, Rosmari Jutemark. She never stopped believing in me and always gave me love and support through all my life. I could never have accomplished anything without you. *Thanks mum, I love you!!*

Bea

7. References

[1] D.W.O. Rogers, B. A. Faddegon, G.X. Ding, C.M. Ma, J. Wei, and T. R. Mackie, BEAM: A Monte Carlo code to simulate radiotherapy treatment units, Med. Phys. 22, 503 – 524 (1995).

[2] D.W.O. Rogers, B. Walters, I. Kawrakow. BEAMnrc user's manual. *National Research Council Report PIRS-0509(A)revH* , 2004

[3] B.R.B. Walters and D.W.O. Rogers. DOSXYZnrc User's Manual. *National Research Council Report PIRS-794)revA, 2004*

[4] J.R. Treurniet, B.R. Walters and D.W.O. Rogers. BEAMnrc, DOSXYZnrc and BEAMDP GUI User's Manual. *National Research Council Report PIRS-0623revB, 2001*

[5] J.R. Treurniet and D.W.O. Rogers. EGS_Windows_4.0 User's manual. *National Research Council Report PIRS-0669, 1999*

[6] D. Sheikh-Bagheri, D. W. O. Rogers, C. K. Ross, and J. P. Seuntjens, Comparison of measured and Monte Carlo calculated dose distributions from the NRC linac, Med. Phys. 27, 2256 - 2266 (2000).

[7] D. Sheikh-Bagheri and D. W. O. Rogers, Sensitivity of megavoltage photon beam Monte Carlo simulations to electron beam parameters, Med. Phys. 29, 379 - 390 (2002).

[8] D. Sheikh-Bagheri and D. W. O. Rogers, Monte Carlo calculation of nine megavoltage photon beam spectra using the BEAM code, Med. Phys. 29, 391 - 402 (2002).

[9] George X Ding. Energy spectra, angular spread, fluence profiles and dose distributions of 6 and 18 MV photon beams: results of Monte Carlo simulations for Varian 2100EX accelerator, Phys. Med. Biol. 47 (2002) 1025-1046

[10] P. Andreo and A.E. Nahum, Spopping-power ratio for a photon spectrum as a weighted sum of the values for monoenergetic photon beams, Phys. Med. Biol. 30, 1055-1065 (1985)

[11] S. H. Cho, O. N. Vassiliev, S. Lee, H. H. Liu, G. S. Ibbott and R. Mohan, Reference photon dosimertry data and reference phase space data for the 6 MV photon beam from a Varian Clinac 2100 series linear accelerators, Med. Phys. 32 (1) January 2005.

[12] Emily Heath and Jan Seuntjens, Development and validation of a BEAMnrc compartment module for accurate Monte Carlo modeling of the Varian dynamic Millennium multileaf collimator. Phys. Med. Biol. 48 (2003) 4045-4063

[13] J. Van de Walle, C. Martens, N. Reynaert, H. Palmans, M. Coghe, W. De Neve, C.De Wagter and H.Thierens. Monte Carlo model of the Elekta SL*i*plus accelerator: validation of a new MLC component module in BEAM for a 6 MV beam. Phys.Med. Biol. 48 (2003) 371-385

[14] Jun Deng, Steve B. Jiang, Ajay Kapur, Jinsheng Li, Todd Pawlicki and C-M Ma. Photon beam characterization and modeling for Monte Carlo treatment planning. Phys. Med. Biol. 45 (2000) 411-427.

[15] D. M. J. Lovelock, C. S. Chui, and R. Mohan, A Monte Carlo model of photon beams used in radiation therapy, Med. Phys. 22, 1387 – 1394 (1995).

[16] C-M. Ma, E. Mok, A. Kapur, T. Pawlicki, D. Findley, S. Brain, K. Forster, A. L. Boyer, Clinical implementation of a Monte Carlo treated planning system. Med. Phys. 26(10) 2133-2144 (oct 1999)

[17] J. Yang, J S Li, L Qin, W Xiong and C-M Ma, Modelling of electron contamination in clinical photon beams for Monte Carlo dose calculations, Phys. Med. Biol. 49 (2004) 2657-2673.

[18] E Spezi, D G Lewis and C W Smith, A DICOM-RT-based toolbox for the evaluation and verification of radiotherapy plans. Phys. Med. Biol. 47 (2002) 4223-4232

[19] George X Ding, Using Monte Carlo simulations to commission photon beam output factors – a feasibility study. Phys. Med. Biol. 48 (2003) 3865-3874

[20] George X Ding, Chryl Duzenli, Nina I Kalach, Are neutrons responsible for the dose discrepancies between Monte Carlo calculations and measurements in the build-up region for high-energy photon beam? Phys. Med. Biol. 47 (2002) 3251-3261

[21] Frank H. Attix, Introrduction to radiological physics and radiation dosimetry. "A Wiley-Interscience publication", John Wiley & Sons, Inc, (1986)

[22] P. J. Keall, J. V. Siebers, B. Libby and R. Mohan, Determining the incident electron fluence for Monte Carlo-based photon treatment planning using a standard measured data set, Med. Phys. 30 (4), April 2003

[23] C. L. Hartmann Siantar, R. S. Walling, T. P. Daly, B. Faddegon, N. Albright, P. Bergstrom, A. F. Bielajew, C. Chuang, D. Garrett, R. K. House, D. Knapp, D. J. Wieczorek and L. J. Verhey, Description and dosimetric verification if the PEREGRINE Monte Carlo dose calculation system for photon beams incident on a water phantom, Med. Phys. 28 (7), July 2001.

[24] B. R. B. Walters, I. Kawrakow and D. W. O. Rogers, History by history statistical estimators in the BEAM code system. *National Research Council Report PIRS-0791*(2002)

8. Appendices

8.1 Appendix 1.

Monte Carlo simulation with BEAMnrc/DOSXYZnrc

8.1.1 ECUT and PCUT

ECUT is the global cut-off energy for electron transport (in MeV, including rest mass), below which the electron's history is terminated and the energy deposited in the current region. This means that in a simulation where ECUT is chosen to be 0,521 MeV the electrons with kinetic energy below 0,010 keV will be discarded and its energy locally deposited. A rule of thumb is that ECUT should be selected so that its range is one third of the smallest dimension in the dose scoring area. A larger ECUT will speed up the simulation but will reduce the calculation accuracy.

PCUT is the global cut-off energy for photon transport, below which the photon's history is disregarded and its energy locally deposited.

8.1.2 Variance reduction

To speed up the simulation there are some different variance reduction techniques available in BEAMnrc: Range rejection, Bremsstrahlung splitting and Forced interactions. Forced interactions are not used in these simulations.

Range rejection in BEAMnrc

Range rejection is a variance reduction method which terminates a charged particle history if its remaining energy (range) is not sufficient to leave the current region. ESAVE is a variable (in MeV) defining the maximum energy of the charged particle at which range rejection is considered. A subroutine in BEAMnrc pre-calculates the residual range of the charged particles in each region.

Range rejection introduces an approximation. It assumes that any bremsstrahlung photons created by the charge particle slowing down would not leave the current region or reach the scoring plane at the bottom of the accelerator. The effect of this approximation is minimized by ESAVE allowing charged particles with insufficient energy to leave the region to still be able to create bremsstrahlung photons exiting the region. The appropriate selection of ESAVE is dependent on the situation. It has been shown that with ESAVE = 2 MeV only 0.1 % of photons reaching the phantom surface are ignored [6].

ESAVE_GLOBAL is treated internally except for the CM SLABS since it is often used as a bremsstrahlung target and where more control is wanted.

Bremsstrahlung Splitting in BEAMnrc

Bremsstrahlung Splitting is a variance reduction technique which increases the number of bremsstrahlung photons created in the target. Each created bremsstrahlung photon produces N bremsstrahlung photons which are sampled individually and with their weight reduced to 1/N times the weight of electron that underwent the bremsstrahlung event. The energies and directions of each photon are sampled individually according to the relevant probability distributions.

8.1.3 Simulation parameters in BEAMnrc

The parameters for the BEAMnrc simulation were: ECUT = 0.521 MeV, PCUT = 0.010 MeV, photon interaction forcing turned off, no Rayleigh scattering, Selective Bremsstrahlung Splitting (SBS) with N_{min} = 10 and N_{max} = 200, Russian roulette turned off and Range rejection with ESAVE_GLOBAL = 1 MeV. Range rejection was turned off for the target to provide the most accurate model for bremsstrahlung production.

Cross-section data for the specific materials in the accelerator were from the PEGS4 file 521icru.pegs4dat. This data file contains cross-section data for particles with kinetic energy down to 10 keV and densities for all the different materials used in the accelerator.

8.1.4 Simulation parameters in DOSXYZnrc

The parameters for the DOSXYZnrc simulation were: ECUT = 0.6 MeV and PCUT = 0.010 MeV. No variance reduction techniques, such as range rejection and photon splitting, were used and the 521icru.pegs4dat was used as input file for cross-section data.

8.1.5 Time saving with variance reduction

The simulation with 18 MV photon beam 40 x 40 cm^2 field was initially performed with neither range rejection nor bremsstrahlung splitting. Simulations of 160 million electrons at the target produced approximately 32 million particles in the phase-space file and took about 65 hours.

The same simulation applying range rejection (ESAVE = 1 MeV) and selective bremsstrahlung splitting (N_{min} = 10, N_{max} = 200) took only about 30 minutes and required 1 million electrons at the target to produce about 38 million particles in the phase space file. This simulation was hence approximately 130 times faster than the one without variance

reduction. The variance reduction technique that was shown to be the most timesaving in the calculations was photon splitting. The range rejection speeds up the simulation with approximately a factor of 4.

To ensure that the energy fluence was not changed due to variance reduction, the two phase-space files were investigated with BEAMDP. No effects of the variance reduction were discovered.

8.1.5 Simulations on the cluster

A state-of-the art cluster of 13 computers connected in parallel, each with a 2.6 MHz Intel Pentium 4 processor, was used to reduce the calculation time.

The simulation splits up between the 13 PCs and makes the simulation 13 times faster than if only one PC was used. The original input file splits up into an arbitrary number of input files each with a unique pair of seeds, a number between 1 and 31328 and 1 and 30081 respectively. For each different pair of seeds, an independent random number sequence is generated. At the end of the simulation the output files has to be collect and combined into one. Simulating the accelerator with BEAMnrc on the cluster will give an arbitrary number of different phase-space files that has to be combined into one. Similarly when simulating dose distributions in a water phantom with DOSXYZnrc the dose distribution files have to be combined into one file.

8.2 Appendix 2.

Phase-space file analysis

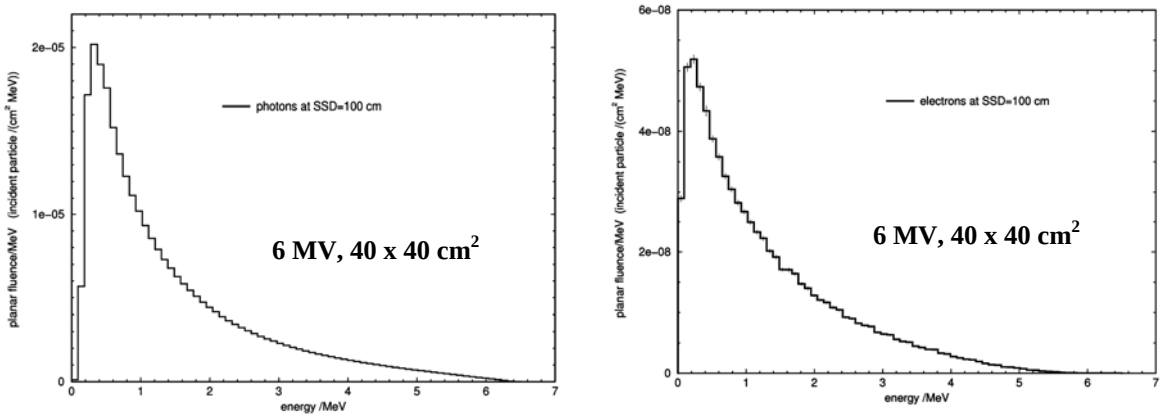

Figure 19. Energy spectra of photons (fig. to the left) and electrons (fig. to the right) at the phantom surface and inside the 40 x 40 cm^2 field for a 6 MV photon beam.

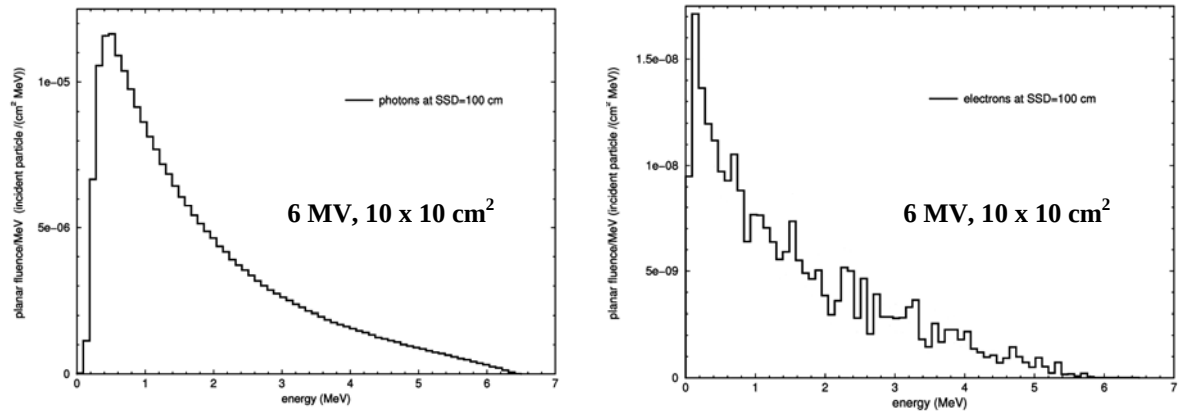

Figure 20. Energy spectra of photons (fig. to the left) and electrons (fig. to the right) at the phantom surface and inside the 10 x 10 cm^2 field for a 6 MV photon beam.

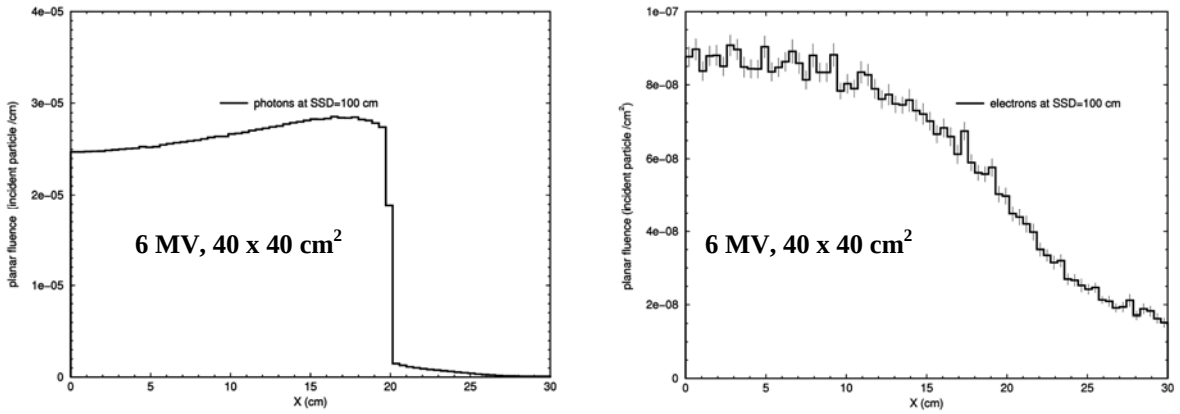

Figure 21. Planar fluence profiles of photons (fig. to the left) and electrons (fig. to the right) at the phantom surface of a 40 x 40 cm^2 field at 6 MV (SSD = 100 cm).

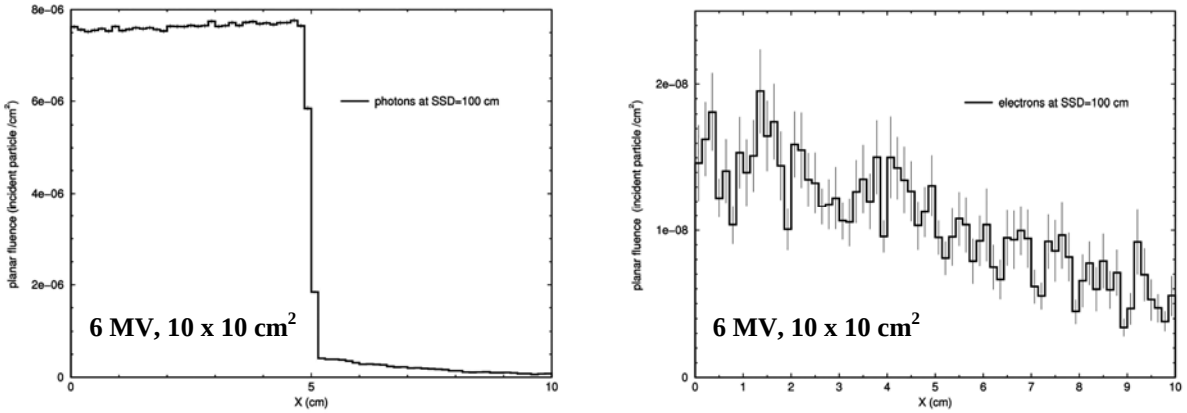

Figure 22. Planar fluence profiles of photons (fig. to the left) and electrons (fig. to the right) at the phantom surface of a 10 x 10 cm^2 field at 6 MV (SSD = 100 cm).

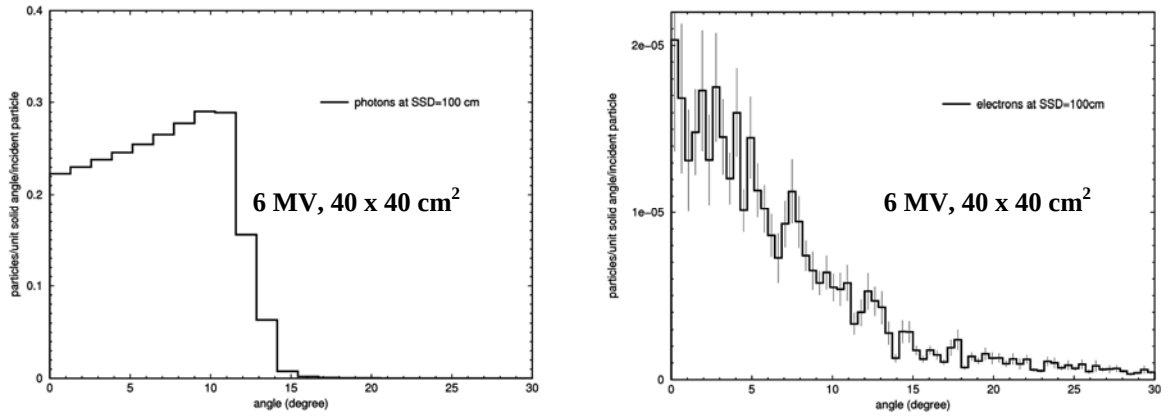

Figure 23. Angular distribution for the photons (fig. to the left) and electrons (fig. to the right) at the phantom surface of a 40 x 40 cm^2 field at 6 MV (SSD = 100 cm).

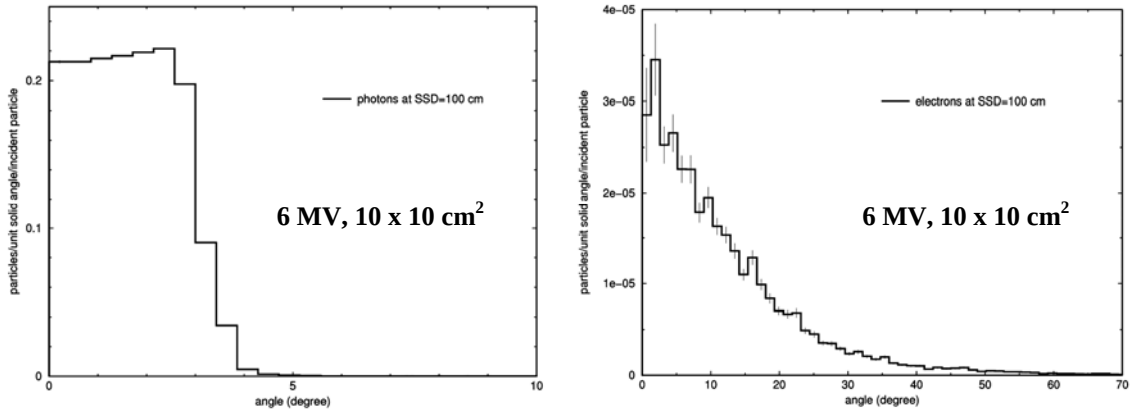

Figure 24. Angular distribution for the photons (fig. to the left) and electrons (fig. to the right) at the phantom surface of a 10 x 10 cm^2 field at 6 MV (SSD = 100 cm).

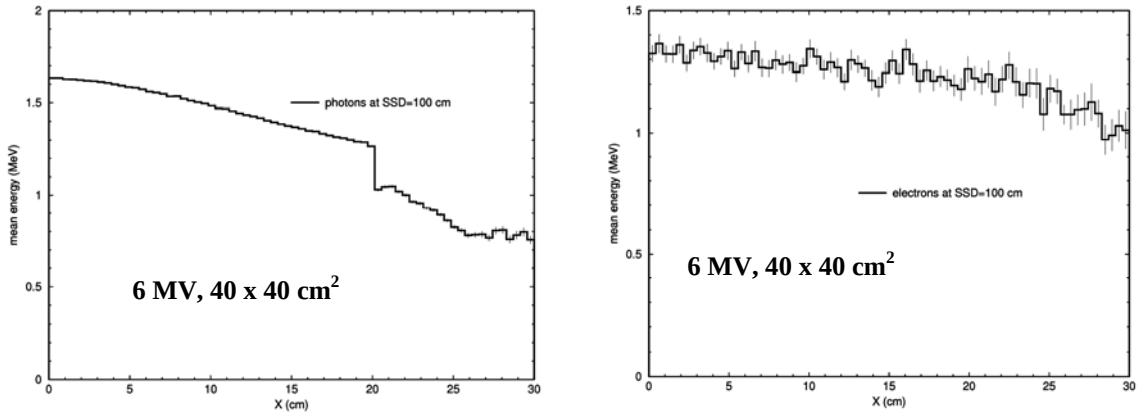

Figure 25. Mean energies for the incident photons (fig. to the left) and electrons (fig. to the right) at the phantom surface as a functions of off axis distance for a 40 x 40 cm^2 field at 6 MV (SSD = 100 cm).

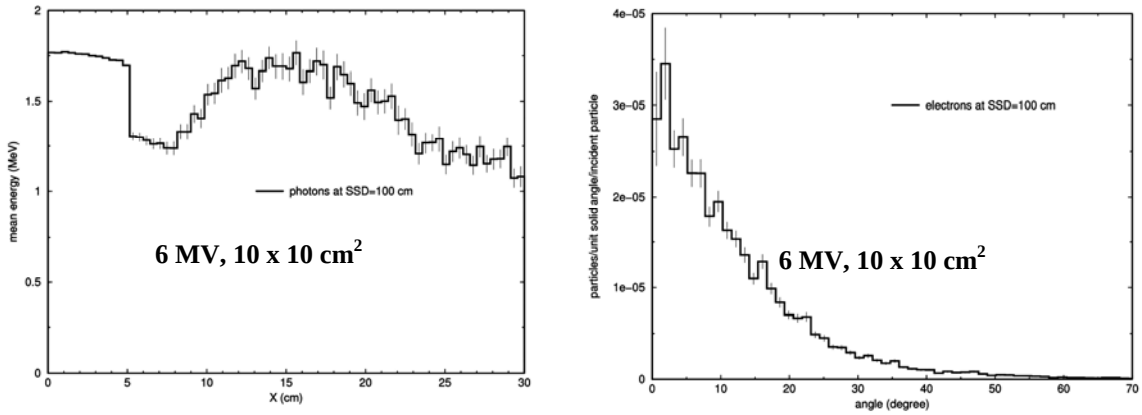

Figure 26. Mean energies for the incident photons (fig. to the left) and electrons (fig. to the right) at the phantom surface as a functions of off axis distance for a 10 x 10 cm^2 field at 6 MV (SSD = 100 cm).

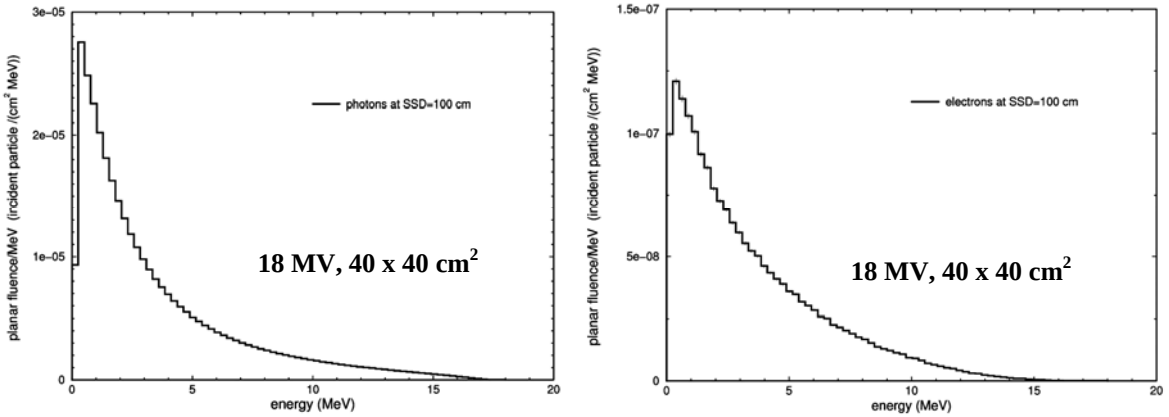

Figure 27. Energy spectra of photons (fig. to the left) and electrons (fig. to the right) at the phantom surface and inside the 40 x 40 cm^2 field of an 18 MV photon beam.

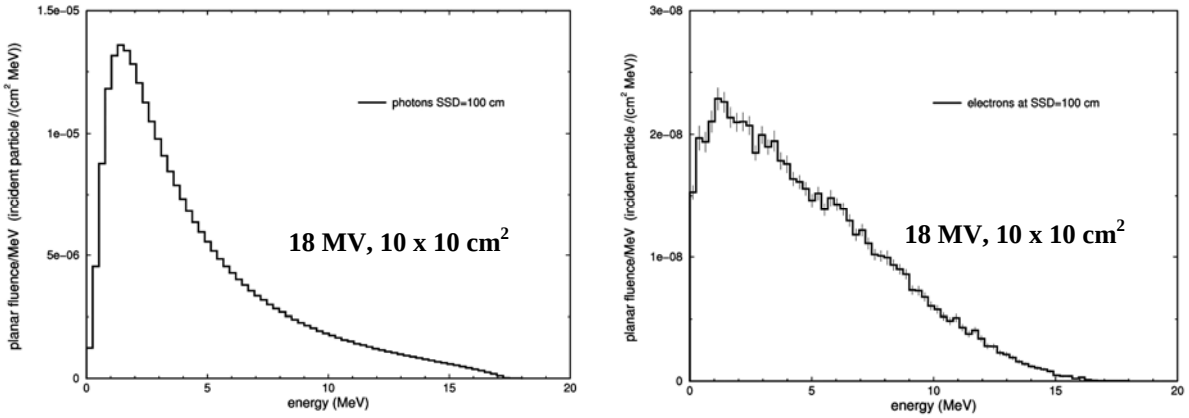

Figure 28. Energy spectra of photons (fig. to the left) and electrons (fig. to the right) at the phantom surface and inside the 10 x 10 cm^2 field of an 18 MV photon beam.

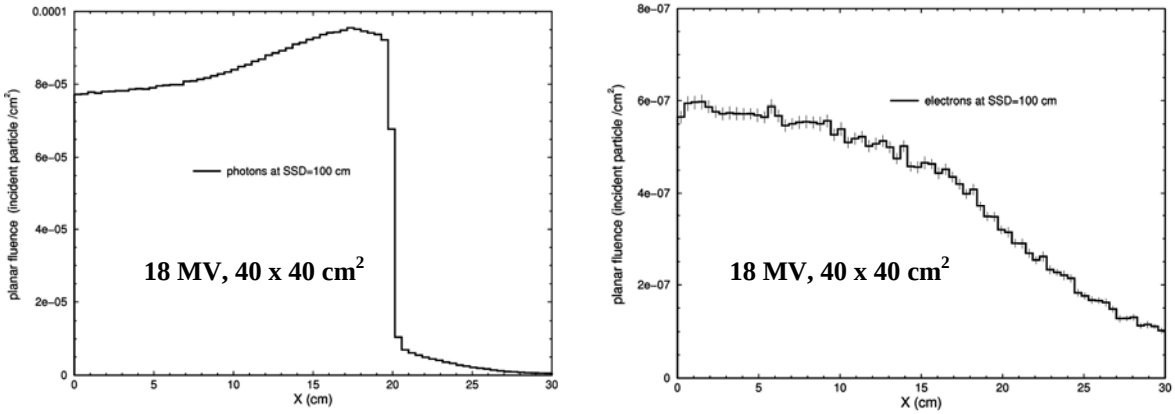

Figure 29. Planar fluence profiles of photons (fig. to the left) and electrons (fig. to the right) at the phantom surface of a 40 x 40 cm^2 field at 18 MV (SSD = 100 cm).

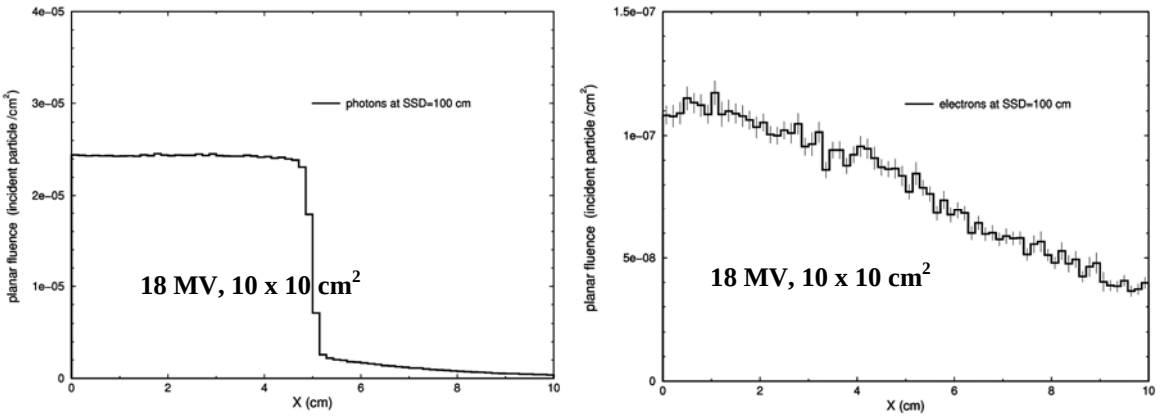

Figure 30. Planar fluence profiles of photons (fig. to the left) and electrons (fig. to the right) at the phantom surface of a 10 x 10 cm^2 field at 18 MV (SSD = 100 cm).

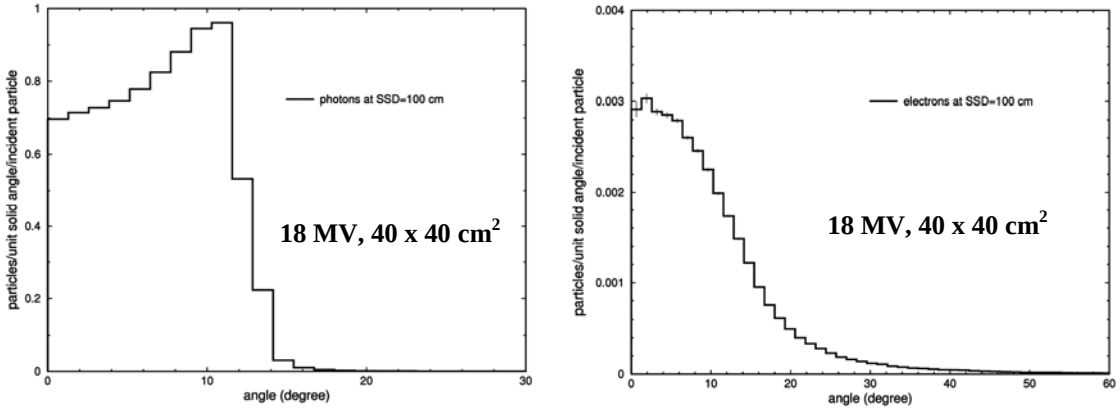

Figure 31. Angular distribution for the photons (fig. to the left) and electrons (fig. to the right) at the phantom surface of a 40 x 40 cm^2 field at 18 MV (SSD = 100 cm).

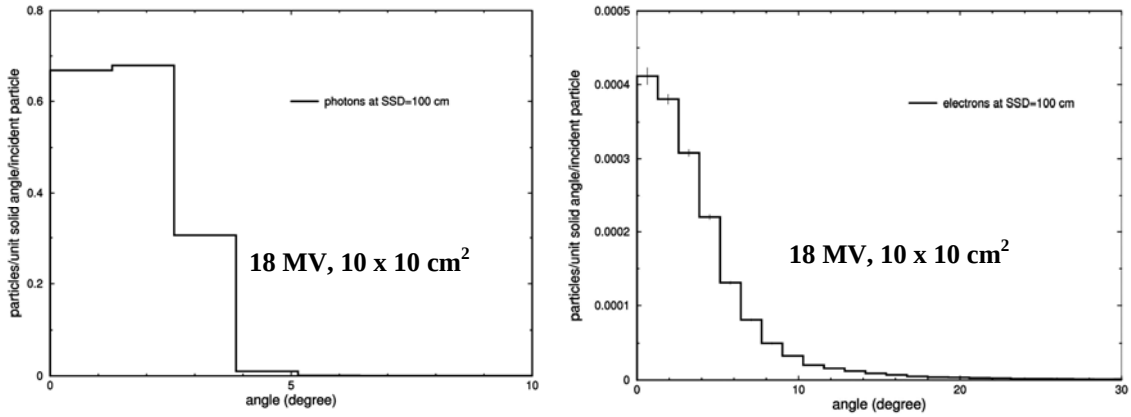

Figure 32. Angular distribution for the photons (fig. to the left) and electrons (fig. to the right) at the phantom surface of a 10 x 10 cm^2 field at 18 MV (SSD = 100 cm).

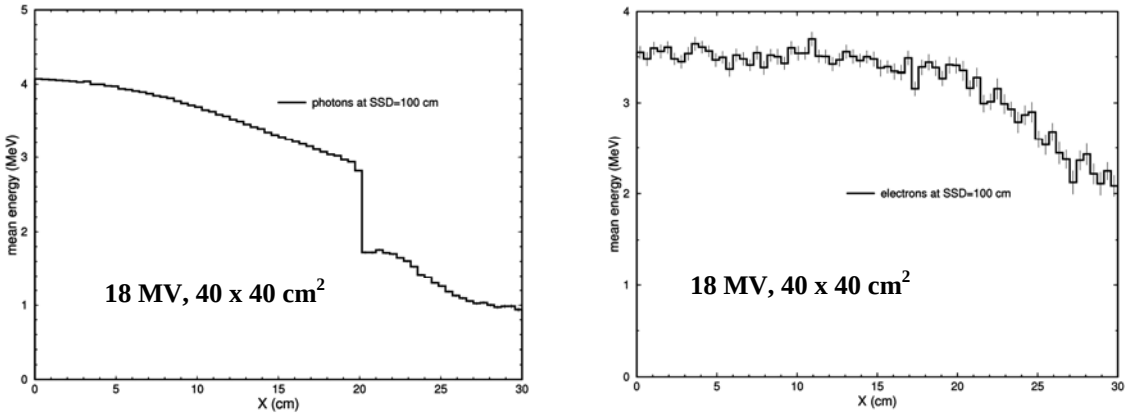

Figure 33. Mean energies for the incident photons (fig. to the left) and electrons (fig. to the right) at the phantom surface as a functions of off axis distance for a 40 x 40 cm^2 field at 18 MV (SSD = 100 cm).

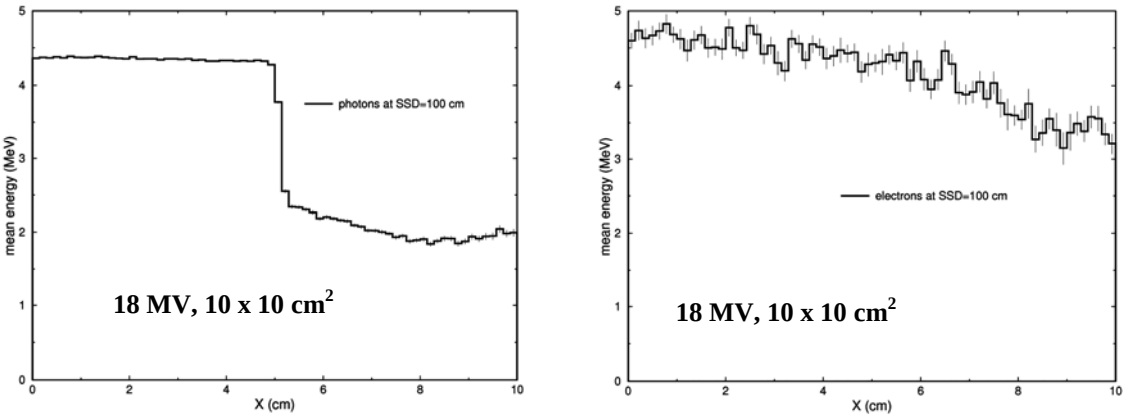

Figure 34. Mean energies for the incident photons (fig. to the left) and electrons (fig. to the right) at the phantom surface as a functions of off axis distance for a 10 x 10 cm^2 field at 18 MV (SSD = 100 cm).

8.3 Appendix 3.

Investigation of the electron beam parameters

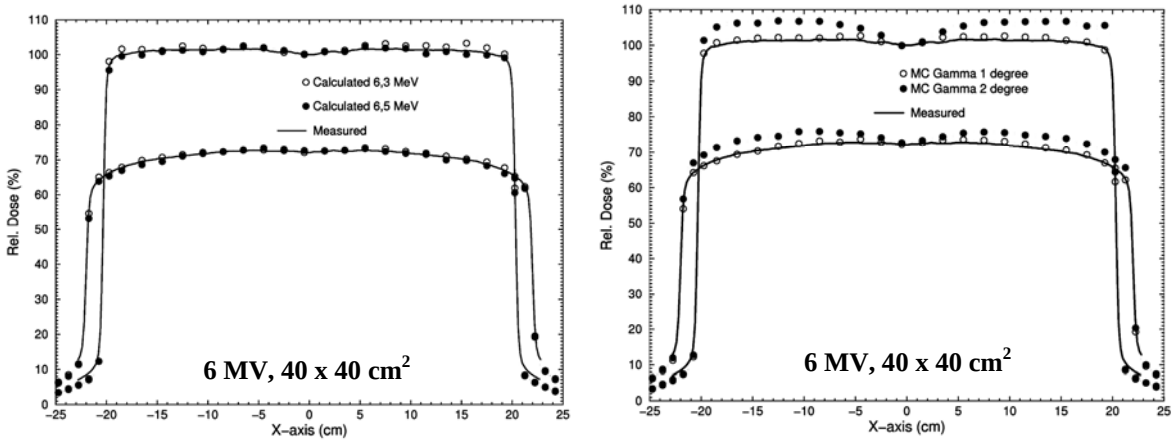

Figure 35. Investigation of mean energy (fig. to the left) and investigation of the angular distribution (fig. to the right) of the incident primary electron beam at the target.

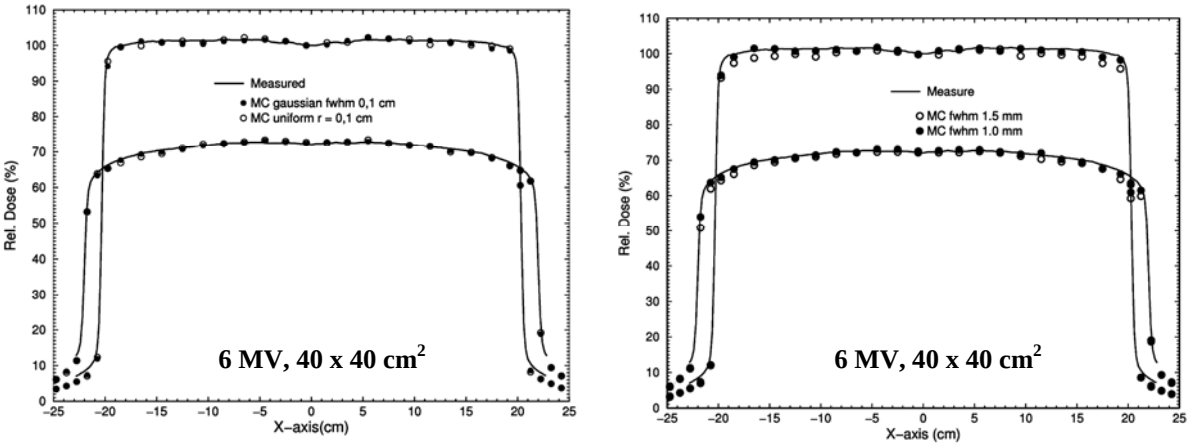

Figure 36. Investigation of the radial intensity distribution of two different radial spreads (fig. to the left) and investigation of the size of the FWHM of a Gaussian spread of the primary electron beam incident at the target.

9. Summary for the general public in Swedish

9.1 Monte Carlo simulering av strålbehandlingsapparat – kasta tärning med fotoner

Många av dagens cancerpatienter får strålbehandling. Den strålning som produceras i en strålbehandlingsapparat är av två olika slag: elektronstrålning och fotonstrålning. Vanligt ljus är också fotonstrålning, men fotonstrålningen som används inom strålbehandling är mycket mer energirik och kallas med ett annat namn för röntgenstrålning. Inför en strålbehandling görs mycket planering utav ett team bestående av bl.a. läkare, sjuksköterskor och sjukhusfysiker. Med hjälp av avancerade tredimensionella dosplaneringssystem beräknas dosfördelningen i patienten. Dosplaneringssystemen använder sig utav matematiska algoritmer. Men med dessa program blir inte stråldosen korrekt beräknad i gränsen mellan vissa områden av olika densitet (t.ex. mellan olika organ). Detta skapar problem vid vissa behandlingstekniker som används.

Ett så kallat Monte Carlo program har använts i denna studie för att undersöka fotonstrålningen från en strålbehandlingsapparat på Rigshospitalet i Köpenhamn. Den information om fotonstrålningen, som man kan få genom såkallade Monte Carlo simuleringar, kan man så småningom använda för att utveckla bättre dosplaneringssystem. Man kan säga att ett Monte Carlo program fungerar som en slumpgenerator som genomför sannolikhetsbaserade beräkningar. Ett Monte Carlo program bygger på den verkliga strålningsfysiken och behandlar varje partikel i en stråle för sig.

Röntgenfotoner skapas genom att elektroner med mycket hög energi (hög hastighet) träffar ett såkallat ”target”. Target sitter i huvudet på strålbehandlingsapparaten och är gjort av ett ämne med högt atomnummer. Fotonstrålningens karaktäristik beror på den elektronstråle som träffar target. I denna studie skulle bl.a. elektronstrålens energi, dess energispridning, intensitets fördelning och dess vinkelfördelning bestämmas med hjälp av Monte Carlo simuleringar. Det Monte Carlo program som användes i denna studie heter BEAMnrc/DOSXYZnrc. I BEAMnrc kan man bygga en virtuell strålbehandlingsapparat med alla dess väsentliga komponenter och i DOSXYZnrc kan man beräkna dosfördelningen i t.ex. vatten. Genom att simulera många miljoner partiklar kan man få en bild utav dosfördelningen.

När man gör små ändringar på den inkommande elektronstrålens olika parametrar kan man få en förståelse för hur dessa olika parametrar påverkar dosfördelningen i vatten. I denna studie skulle elektronstrålens olika parametrar bestämmas genom att matcha beräknade och experimentella dosfördelningar för två olika fotonenergier, 6 MV och 18 MV, som den undersökta strålbehandlingsapparaten har. Man kom fram till att fotonstrålen generades utav en elektronstråle med Gaussisk intensitets fördelning med bredden 1.2 och 1.5 mm, och med energin 6.4 MeV och 17.5 MeV, för att producera fotonstrålning med 6 MV respektive 18 MV. Med denna information om elektronstrålen kan man göra dosplaneringar med hjälp av Monte Carlo simuleringar där dosfördelningen är korrekt, även i gränser mellan områden av olika densitet.